Desalination and Water Treatment
www.deswater.com
41 (2012) 131–169
March
1944-3994/1944-3986 © 2012 Desalination Publications. All rights reserved
doi: 10.1080/19443994.2012.664698
Taylor & Francis
Taylor & Francis Group

Degradation of wastewaters containing organic dyes photocatalysed by zinc oxide: a review

Sze-Mun Lam, Jin-Chung Sin, Ahmad Zuhairi Abdullah, Abdul Rahman Mohamed*

School of Chemical Engineering, Universiti Sains Malaysia, Engineering Campus, 14300 Nibong Tebal, Pulau Pinang, Malaysia
Tel. +60 45996410; Fax: +60 45941013; email: chrahman@eng.usm.my

Received 4 July 2011; Accepted 15 January 2012

ABSTRACT

Organic dyes are one of the largest groups of pollutants discharged into wastewaters from textile and other industrial processes. Owing to the potential toxicity of the dyes and their visibility in surface waters, removal and degradation of them have attracted considerable attention worldwide. A wide range of approaches have been developed, amongst which the heterogeneous photocatalysis involving zinc oxide (ZnO) emerges as a promising new route for water purification process. For the first time, we attempt to review and summarize the recent research on ZnO photocatalytic systems for organic dyes degradation. The photocatalysis on modified ZnO is also discussed, in particular aiming at enhancing the degradation efficiency and activity in visible region as well as solar irradiation. The effects of key operational parameters on the photocatalytic performance in terms of the degradation and mineralization of dyes are detailed. This review also highlights the utilization of multivariate analysis to determine the optimum operational parameters so as to improve process performance and photodegradation efficiency. Brief discussions on the analysis techniques and identification of reaction intermediates that are generated during dye degradation are presented. Finally, the real-world process scenarios for the potential practical utility of this technique are summarized and discussed.

Keywords: ZnO; Dye; Photocatalysis; Parameter; Multivariate analysis; Intermediates

1. Introduction

With increasing revolution in science and technology, there was a greater demand on opting for newer chemicals which could be used in various industrial activities. Organic dyes are one such of the many new chemicals which could be used in many industrial processes including fabric, woven, leather, textile, pulp and paper, tanneries, cosmetic, pharmaceuticals, food processing, agricultural research, electroplating and distillers. Due to their large-scale production and extensive applications, organic dyes have become an integral part of industrial wastewater. In fact, of the 7×10^5 tonnes of organic dyes annually produced worldwide, more than 10–15% is lost in the wastewater during manufacturing and application processes [1,2]. Wastewater from the dye manufacturing generally contains residual dyestuffs, dye intermediates as well as unreacted raw materials such as aromatic amines and inorganic sodium salts. Waste streams being variable in composition and strength are produced at different stages of the dye manufacturing process. The wastewater is commonly characterized by its high chemical oxygen demand (COD), strong

*Corresponding author.

colour, total dissolved solids (TDS) content, variable pH and low biodegradability, implying the presence of recalcitrant organic matter [3]. Dyes and their intermediates can undergo reductive processes and result in the formation of potentially carcinogenic or mutagenic compounds and detrimental impact towards the survival of microorganisms, aquatic life and environmental matrix (water and soil) [4]. The ingestion of such contaminated water in the human body may also be susceptible to a broad spectrum of immune-suppression, respiratory, central nervous, neurobehavioural disorders presage as allergy, tissue necrosis, eye (or skin) infections and irritation and even lung edema [5].

Various physical, chemical and biological treatments have been widely used to handle the dye removal from wastewaters in order to comply with the environmental regulations, which are becoming more stringent these days. Physical and biological treatments have been successfully applied till now but these methods have their own drawbacks. The aerobic treatment process is associated with the formation and disposal of large amounts of biological sludge, while wastewater treated by anaerobic treatment method does not lower down the pollutant contents to a satisfactory level. Activated charcoal adsorption and air stripping methods are non-destructive, since they simply transfer the pollutants from water to another phase. They either transfer it to the atmosphere, which causes air pollution, or to a solid which is often disposed off in landfills or must be needed to regularly regenerate the adsorbent materials [6]. Merely transferring toxic materials from one phase to another is not a long term goal to achieve better management and elimination of the hazardous waste loading to the environment. In recent years an alternative to conventional methods, is "advanced oxidation processes" (AOPs) based on the *in situ* generation of non-selective and highly reactive species such as hydroxyl radicals (·OH), superoxide anion radicals (O_2^{-}) and hydrogen peroxide (H_2O_2) as initiators of the oxidative degradation [7,8]. Among AOPs, heterogeneous photocatalysis seems to be an attractive method as it has been successfully employed for the degradation of various families of organic pollutants, including the dyes. Heterogeneous photocatalysis is a process in which the degradation of organic pollutants is governed by the combined actions of a semiconductor catalyst, an emitted light and an oxidizing agent. The semiconductor catalysts usually are oxides that can be more appealing than the conventional chemical oxidation methods because semiconductors are low cost, nontoxic and capable of extended use without substantial loss of photocatalytic activity [9].

Another reason for the increased interest on the photocatalysis application is that the process has the potential to utilize solar UV and visible lights. In countries such as Malaysia where ample amount of sunlight is available, using sunlight to execute photocatalysis will be economical and favourable as solar light contains about 42% visible and 5% UV light, which is free and inexhaustible. Nevertheless, the application of semiconductor catalysts for wastewater treatment is still experiencing a series of technical challenges. These include in the catalyst development with broader photoactivity range in the visible light region as well as solar light spectrum. The understanding of the theory behind the common operational parameters and their interactions is also insufficient and presents a difficult task for process optimization. Such understanding on the role of these operational parameters is highly crucial from the perspective of efficient design and application of photocatalytic processes to ensure sustainable operation in wastewater treatment. Other technical challenges include the lack of suggestive analysis techniques and intermediates detection for a large variety of organic pollutants. In addition, most of the research works concerned only over the years on single-constituent model solution remained as the major obstacle towards the practicality as real-world wastewaters are in the form of mixture. With the aforementioned, this review slates to give an overview of the understanding and recent development of photocatalytic organic dyes treatment using ZnO-based catalysts.

Hence, this paper presents a review of recent research on ZnO photocatalytic systems aiming at organic dyes degradation in wastewater treatment. In particular the review focuses on: enhancing the degradation efficiency through modified ZnO, optimizing the various operational parameters in the photocatalytic process, providing insight into the synthesis techniques of ZnO catalyst and improving the detection of degradation intermediates via numerous analysis techniques. A short outlines of the real-world process scenario and future research for the feasible applications of ZnO wastewater treatment are also discussed.

1.1. Classification of organic dyes

To better understand the complex structure of organic dyes in terms of their treatment, a brief review of dyes in general and their structures in particular are presented. Organic dyes contain two key components: the chromophores, delocalized electron systems with conjugated double bonds and the auxochromes, electron-withdrawing or electron-donating substituents that intensify the colour of the chromo-

phore by altering the overall energy of the electron systems. Usual chromophores are –C=C–, –C=N–, –C=O, –N=N–, $–NO_2$ and quinoid rings, while the auxochromes are $–NH_3$, –COOH, $–SO_3H$ and –OH groups. Depending on the chemical structure or chromophore, a plentiful of different groups of dyes can be distinguished. Each different dye is given a colour index (CI) generic name determined by its application characteristics and its colour. The CI discerns different application classes which are as follows [10–12]:

Acid dyes: The largest class of dyes in the CI is acid dyes. Acid dyes are anionic compounds that find their main application in dyeing nitrogen-containing fabrics like wool, polyamide, silk, modified acryl and to some extent for ink-jet printing, leather, paper and cosmetics. They are generally water soluble. Most acid dyes are azo, anthraquinone or triarylmethane, azine, xanthene, nitro and nitroso compounds.

Reactive dyes: Reactive dyes are dyes with reactive groups that are capable of forming a covalent bond between a carbon atom of the dye molecule and –OH, –NH or –SH groups in fibers such as cotton, wool, silk and nylon. Most reactive dyes (~80%) are azo or metal complex azo compounds but also anthraquinone and phthalocyanine reactive dyes are applied. The reactive dyes are a commercially available important class of textile dyes for which loss through processing operations is significant and the treatment is problematic. It is estimated that 10–50% of the dye will not react with the fabric and remains in a hydrolysed or unfixed form in the water phase. The dilemma of coloured effluent is thus primarily due to the utilization of reactive dyes.

Direct dyes: Direct dyes are relatively large molecules used in the dyeing of cotton, rayon, nylon and to some extent to leather and paper. They are water-soluble anionic dyes and when dyed from aqueous solution in the presence of electrolytes have high affinity for cellulose fibers. These dyes are mostly azo dyes with more than one azo bond or phthalocyanine, stilbene or oxazine compounds. In the CI, the direct dyes form the second largest dye class with respect to the amount of different dyes.

Basic dyes: Basic dyes are cationic compounds that are used for dyeing acid-group containing fibers such as modified nylon, modified polyesters and polyacrylonitrile. These water-soluble dyes yield coloured cations in solution and that is why are called as cationic dyes. Most basic dyes are diarylmethane, triarylmethane, anthraquinone or azo compounds.

Mordant dyes: Mordant dyes are fixed to the fabric by the addition of a mordant, a chemical that combines with the dye and the fiber. They are used with wool, leather, silk, paper and modified cellulose fibers. Most mordant dyes are azo, oxazine or triarylmethane compounds.

Disperse dyes: Disperse dyes are scarcely soluble dyes that penetrate synthetic fibers including cellulose acetate, polyester, polyamide and acryl. Disperse dyes form the third largest group of dyes in the CI. They are usually small azo or nitro compounds, anthraquinones or metal complex azo compounds.

Solvent dyes: Solvent dyes are non-ionic dyes that are used for dyeing substrates in which they can dissolve like plastics, varnishes, inks, waxes and oils. Most solvent dyes are diazo compounds that undergo some molecular rearrangement. Additionally, triarylmethane, anthraquinone and phthalocyanine solvent dyes are applied.

Vat dyes: Vat dyes are water-insoluble dyes that are particularly and widely used for dyeing cellulose fibers. Almost all vat dyes are anthraquinones or indigoids.

Besides these, there are some other classes such as sulphur having heterocyclic S-containing groups used for cotton and other cellulosic materials, metal complex having azo groups used for wool, leather, synthetic fibers after pre-treating with metals (usually chromium, copper, cobalt or nickel) and fluorescent brightener having stilbene, pyrazoles, coumarin (COU) and naphthalimides groups used for detergents, soaps, oils, paints, fibers and plastics. Fig. 1 illustrates the classification for several typical dyes showing their chemical structure along with their common and/or CI name.

Overall at present, azo dyes represent the largest class of organic dyes listed in the CI (65–70% of the total dyes) and their relative share among reactive, acid and direct dyes is even higher, it can be expected that they make up the vast majority of the dyes discharged by textile processing industries [13]. Anthraquinone dyes are the second largest class, followed by triarylmethanes and phthalocyanines of the entries in the CI. Moreover, reactive dyes are known to form a covalent bond with the fiber in the dyeing process. This leads to favourable properties such as wash-fastness. However, unfixed dye reacts with water to form hydrolysed or oxo-dye intermediate that has lost its bonding capacity and thus cannot be reused. Consequently, dye recovery is not an option with reactive dyes and the treatment process must lead to final destruction or disposal of these organic pollutants.

2. ZnO photocatalyst

ZnO is an oxidic compound naturally occurring as the rare mineral zincite, which crystallizes in three different structures: wurtzite, zincblende and rocksalt. It usually appears as a white powder, nearly insoluble in water but soluble in acids and alkalis. The ZnO is

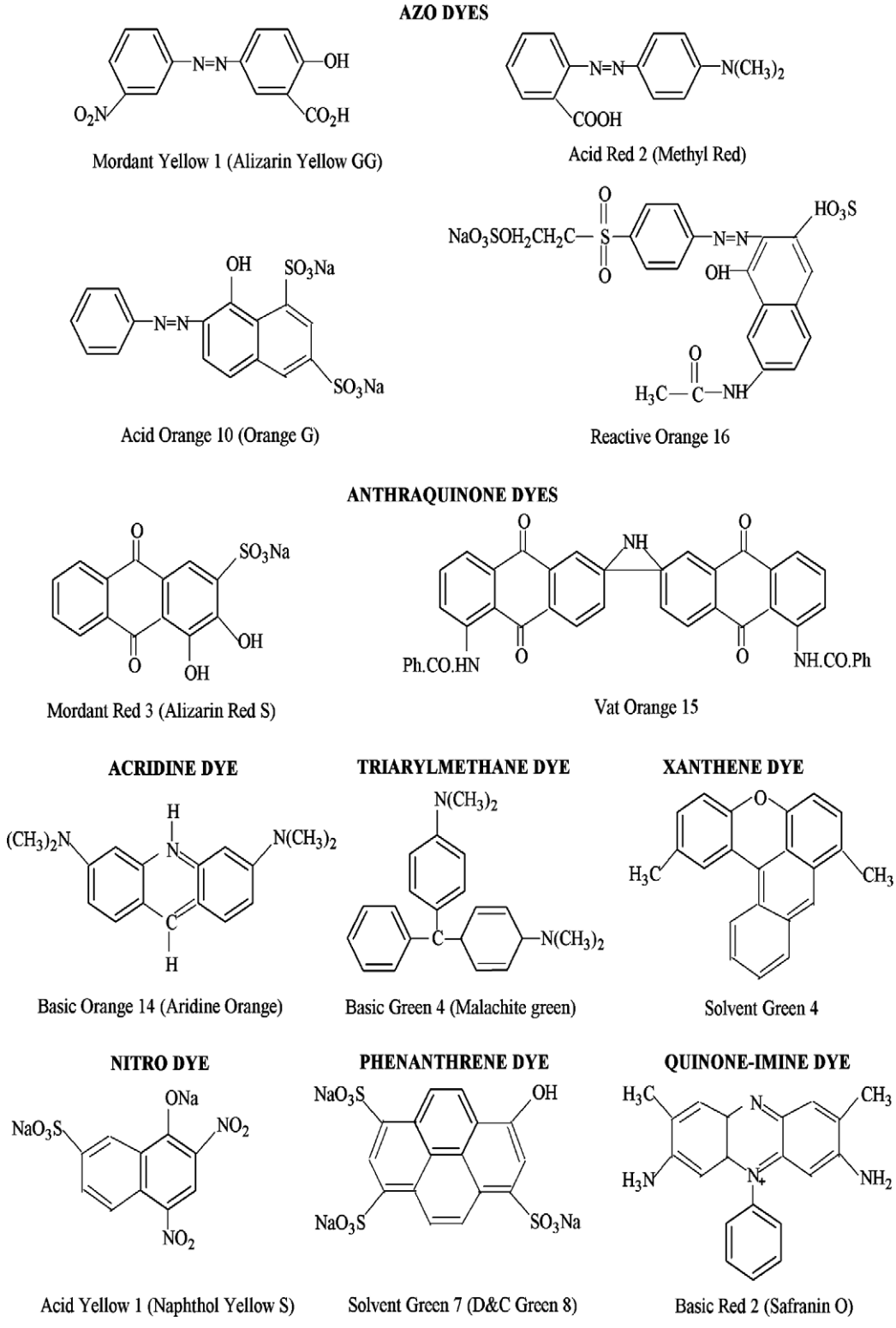

Fig. 1. Chemical structure of various organic dyes classified by their chromophore group. The colour index and/or common (between parentheses) name of each dye are given.

the most frequently used among the zinc compounds and commercially produced using French process—the metallic zinc is vapourized in a large container by external heating. In an adjoining off-take pipe or combustion chamber, the vapour is burned off in the air to a fine ZnO powder [14] and American process—oxidized ores of roasted sulfide concentrates are mixed with anthracite coal (carbon additive) and smelted in a furnace. The coal together with the products of partial combustion mainly carbon monoxide reduced the ore to metallic zinc, which is released as vapour. The zinc vapour is then re-oxidized by lower temperature air and forms ZnO particulate. The purity of the ZnO produced by this process is normally rather inferior to that from the French process as it contains low levels of lead and sulphur [14,15].

In general, ZnO crystallizes in a hexagonal wurtzite structure (Fig. 2a) with lattice parameters $a = 3.25$ Å and $c = 5.20$ Å at ambient pressure and temperature. The structure of ZnO can be simply described as a number of alternating planes composed of tetrahedrally coordinated O^{2-} and Zn^{2+} ions stacked alternately along the *c*-axis. The tetrahedral coordination in ZnO results in piezoelectric and pyroelectric due to the noncentral symmetric structure. Another important characteristic of ZnO is polar surfaces, which are the basal planes $(0\,0\,0\,1)$ and $0\,0\,0\,\bar{1}$). One end of the basal polar plane $(0\,0\,0\,1)$ is terminated by Zn atoms and the other end $(0\,0\,0\,\bar{1})$ is terminated by oxygen atoms. The oppositely charged ions produce positively charged Zn-$(0\,0\,0\,1)$ and negatively charged $O-(0\,0\,0\,\bar{1})$ surfaces, resulting in a normal dipole moment and spontaneous polarization along the *c*-axis as well as a divergence in surface energy. Thus, to maintain electrical neutrality, the polar surfaces typically have facet or exhibit massive surface reconstructions, but not in ZnO ± $(0\,0\,0\,1)$ surfaces that they are atomically flat, stable and with no reconstruction [16,17]. Although the wurtzite structure of ZnO is the thermodynamically stable phase, two other structures of ZnO exist, which are known as the zincblende (Fig. 2b) and the rocksalt (Fig. 2c). These phases are metastable and only occur under certain conditions such as through epitaxial growth of ZnO on a suitable cubic substrate to obtain the zincblende structure, while the rocksalt (NaCl-type) structure is observed when subjected to high pressures (~9 GPa at 300 K) [18]. For this reason, ZnO has a strong natural tendency to crystallize in the wurtzite structure and thus nearly all photocatalytic studies are focused on this structure. Depending on the optical absorption properties, the refractive index of ZnO (2.0) is smaller than that of TiO_2 (2.5–2.7), so ZnO hardly scatters light, thereby making it colourless and enhancing the transparency. In addition, ZnO has a considerably high thermal conductivity of 54 W/m K increases the appeal of ZnO as a substrate for homoepitaxy or heteroepitaxy [19].

ZnO and other semiconductors such as TiO_2, WO_3, ZrO_2, SnO_2, Fe_2O_3, CdS, ZnS, WS_2 and MoS_2 have been attempted for the photocatalytic degradation of a wide variety of environmental contaminants. According to the thermodynamic point of view, the pre-requisite for an efficient semiconductor catalyst is that the valence band and conduction band (CB) of the catalyst should be positioned in such a way that, the oxidation potential of the hydroxyl radical (E^o (H_2O/·OH) = 2.8 V vs. NHE) and the reduction potential of superoxide radical (E^o ($O_2/O_2^{\cdot-}$) = −0.28 V vs. NHE) lie well within the band gap [20]. Table 1 illustrates the

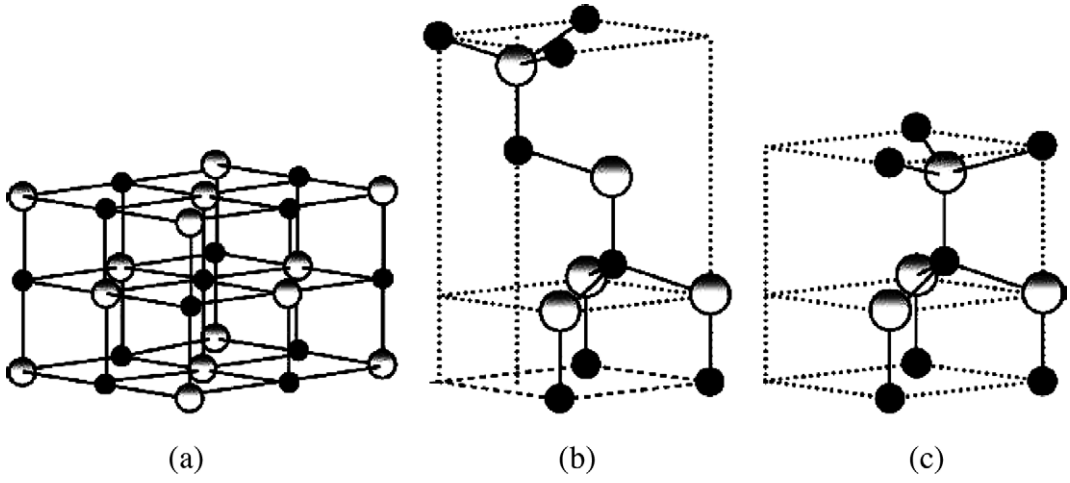

Fig. 2. Stick and ball representation of ZnO crystal structures: (a) cubic rocksalt; (b) cubic zincblende; (c) hexagonal wurtzite. The shaded white and black spheres denote Zn and O atoms, respectively [18].

Table 1
The conduction and valence band positions of some common semiconductor catalysts at pH 1

Semiconductor	VB (V vs. NHE ± 0.1 V)	CB (V vs. NHE ± 0.1 V)	E_g (eV)
ZnO	+3.0	−0.2	3.2
TiO_2	+3.1	−0.1	3.2
WO_3	+3.0	+0.2	2.8
ZrO_2	+4.0	−1.0	5.0
Fe_2O_3	+2.9	+0.6	2.3
SnO_2	+4.1	+0.3	3.8
ZnS	+1.4	−2.3	3.7
CdS	+2.1	−0.4	2.5
CdSe	+1.6	−0.1	1.7
GaAs	+1.0	−0.4	1.4

VB, valence band; CB, conduction band; and E_g, band gap energy [21,22].

band positions of various semiconductors and their band gap energy. It is clear that TiO_2, ZnO and ZrO_2 exhibit favourable band gap positions compared to other catalysts. TiO_2 which has a band gap of 3.2 eV is the most preferred catalyst for the photocatalytic treatment of dye wastewater due to its photoactive, inert and corrosion resistant. Analogous to TiO_2, ZnO has a band gap energy of 3.2 eV which is an alternative potential catalyst for degradation of organic pollutants due to its high quantum efficiency, however, it photocorrodes in acidic aqueous suspensions and suffers dissolution to form $Zn(OH)_2$ on the catalyst surface [20]. Some of the most recent experimental results have shown that ZnO actually exhibited higher photocatalytic activities than TiO_2 and other semiconductor catalysts such as CdS, WO_3, Fe_2O_3, SnO_2 and ZrO_2 especially for degradation of dyes in aqueous solution [23–26]. CdS, WO_3 and Fe_2O_3 with smaller band gap in which the photogenerated electron in these semiconductors rapidly fell into the photogenerated hole and thus showed reduced activity. Many authors have also reported that low band gap semiconductors suffered from limited photoactivities and lacked reproducibility [23,25,26]. Though SnO_2 and ZrO_2 are stable and non-corrosive, they exhibited less photoactivity because the light energy was not sufficient to excite these catalysts with a wide band gap energy. In addition, ZnO is a low cost material, which gives it an additional advantage. Nevertheless, the solar UV-light reaching the earth's surface is relatively small (about 4%) to activate the TiO_2, and artificial UV light sources are rather expensive. The greatest advantage of ZnO is that it absorbs over a larger portion of the solar spectrum than TiO_2 [23].

2.1. Principle of ZnO photocatalysis and mechanistic pathways

Heterogeneous photocatalysis has an increase in the rate of a thermodynamically allowed ($\Delta G < 0$) reaction in the presence of photocatalyst with the increase originating from the creation of some new reaction pathways involving photogenerated species and a decrease of the activation energy [27,28]. Generally, there are four essential key steps in the mechanism of heterogeneous photocatalysis on the surface of ZnO, namely the (1) charge-carrier generation, (2) charge-carrier trapping, (3) charge-carrier recombination and (4) photocatalytic degradation of organic pollutants [29–36].

2.1.1. Charge-carrier generation

Upon irradiation of ZnO with UV light energy of equivalent or greater than its band gap energy, the electron is excited from the valence band to the CB. Fig. 3 illustrates the mechanism of electron–hole pairs generation when the ZnO particle is irradiated with sufficient light energy (hv). The wavelength for UV light energy typically corresponds to $\lambda < 387$ nm. The excitation leaves behind a positive hole in the valence band and therefore creating the electron–hole pair (e^-–h^+).

$$ZnO + hv(UV) \rightarrow ZnO(h^+ + e^-) \quad (1)$$

2.1.2. Charge-carrier trapping

The e^-–h^+ pair is trapped by electron and hole scavengers and inhibited from recombination. The positive hole is a strong oxidant which can either directly oxidize adsorbate pollutants or react with electron donors such as water or hydroxyl ions (OH^-) to form hydroxyl radical ($^{\bullet}OH$), which is also a potent oxidizing agent.

$$h^+ + H_2O \rightarrow {}^{\bullet}OH + H^+ \quad (2)$$

$$h^+ + OH^- \rightarrow {}^{\bullet}OH \quad (3)$$

On the other hand, it is important for the trapped electron in the CB to be scavenged by an electron acceptor to suppress its recombination with the trapped hole. One of the efficient electron acceptors is molecular oxygen (O_2). Through the reduction of O_2 with electron, reactive superoxide radical anions ($O_2^{\bullet-}$) are produced. Together with other oxidizing species

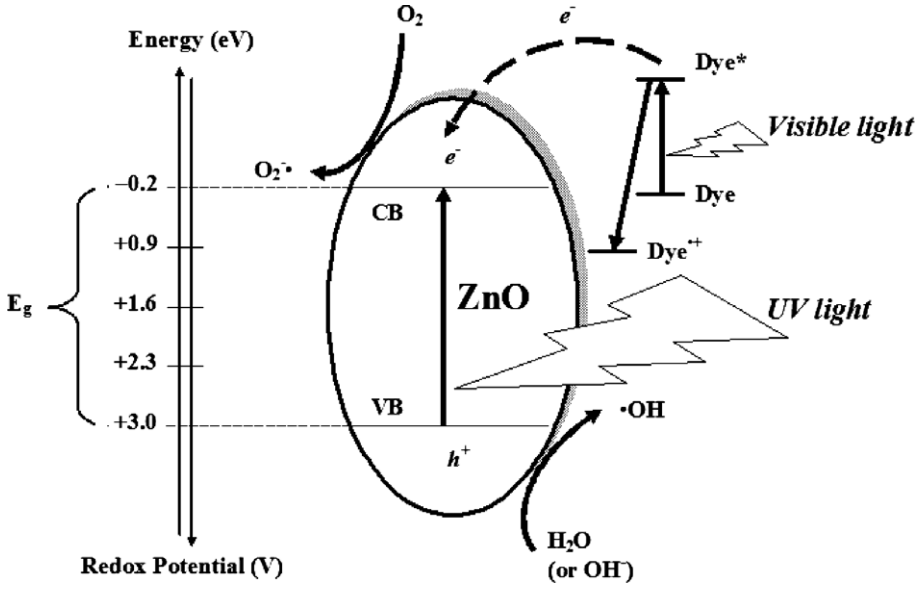

Fig. 3. Schematic diagram illustrating the generation of oxidizing species in ZnO photocatalysis.

such as hydroperoxyl radicals ($HO_2^{\cdot}$) and hydrogen peroxide (H_2O_2) are also subsequently formed. The additional ·OH radicals are generated through the following reactions:

$$O_2 + e^- \rightarrow O_2^{\cdot -} \quad (4)$$

$$O_2^{\cdot -} + H^+ \rightarrow HO_2^{\cdot} \quad (5)$$

$$O_2^{\cdot -} + HO_2^{\cdot} \rightarrow HO_2^{\cdot} + O^- \quad (6)$$

$$2HO_2^{\cdot} \rightarrow H_2O_2 + O_2 \quad (7)$$

$$H_2O_2 + O_2^{\cdot -} \rightarrow OH^- + {}^{\cdot}OH + O_2 \quad (8)$$

$$H_2O_2 + e^- \rightarrow OH^- + {}^{\cdot}OH \quad (9)$$

$$H_2O_2 + hv \rightarrow 2{}^{\cdot}OH \quad (10)$$

2.1.3. Charge-carrier recombination

In competition with charge transfer to adsorbed pollutants, there is the opportunity that both e^-–h^+ pair recombination and trapped carrier recombination happen. This recombination can occur either in the volume of the photocatalyst or on the surface of photocatalyst with a by-product of heat liberation. The characteristic times for various steps in the photocatalysis mechanism have been reported in previous literatures [37,38]. It has been reviewed that the charge-carrier trapping takes place about a nanosecond (100 ps to 10 ns). Charge-carrier recombination exhibits a characteristic time of 10–l00 ns. Interfacial charge transfer of holes is slow (~100 ns) but the slowest step is the interfacial charge transfer of electrons to the electron acceptor (ms).

$$e^- + h^+ \rightarrow ZnO + \text{heat} \quad (11)$$

2.1.4. Photocatalytic degradation

The primary photoreaction (1)–(11) indicated the important role of $e^- - h^+$ pairs in photocatalytic degradation. Essentially, ·OH, $HO_2^{\cdot}$ and $O_2^{\cdot -}$ radicals as well as photogenerated hole (h^+) are highly reactive intermediates that will attack repeatedly in the reacting system and ultimately lead to complete mineralization of the organic pollutants. The mediation of radical oxidative species in the photocatalytic reaction has been evidenced by electron paramagnetic resonance spectroscopy (EPR) using spin trap such as 5,5-dimethylpyrroline-*N*-oxide (DMPO). This process led to the formation of a stable free radical whose EPR spectra were the characteristic of the trapped ·OH radical [39]. Another analysis of the ·OH radical formation on photocatalyst surface in solution has been performed

through simple terephthalic acid–fluorescence (TA–FL) technique. Using this technique, the intensity of the peak attributed to 2-hydroxylterephthalic acid was known to be proportional to the amount of ·OH radicals formed [40,41]. More recently, the ·OH radical produced on various photocatalysts has also been quantitatively investigated by Xiang et al. [42] via photoluminescence (PL) technique using COU as a probe molecule. Furthermore, electron spin resonance (ESR) has been used to study the radical oxidative species detection in solutions. This technique allowed to monitor the presence of ·OH and $HO_2^{\cdot}$ radicals in photocatalytic systems [43–45].

On the contrary, under the visible light at $\lambda > 420$ nm, degradation of dye pollutant has different mechanism pathways (called photosensitized degradation). In photosensitized degradation, the adsorbed dye pollutant is initially excited under visible light irradiation. The excited state dye pollutant can inject electrons into the CB of ZnO particles and then trapped by the surface adsorbed O_2. In the meantime, it is also extremely susceptible for recombination between cationic radicals and the electrons if the injected electrons accumulate in the CB of ZnO particles. Thus, the electrons trapping and electrons transferring become two key steps to suppress the electron–cationic radical recombination. The cationic dye radicals ($Dye^{\cdot+}$) generated by electron injection are less stable than the ground state dye. As a result, unstable cationic dye radicals can directly degrade into their products by reacting with ·OH, $HO_2^{\cdot}$ and $O_2^{\cdot-}$ radicals as follows [46–48]:

$$Dye + h\nu(\mathrm{Vis}) \rightarrow \mathrm{Dye}^* \tag{12}$$

$$\mathrm{Dye}^* + \mathrm{ZnO} \rightarrow \mathrm{Dye}^{\cdot+} + \mathrm{ZnO}(e^-) \tag{13}$$

$$\mathrm{ZnO}(e^-) + \mathrm{O_2} \rightarrow \mathrm{ZnO} + O_2^{\cdot-} \tag{14}$$

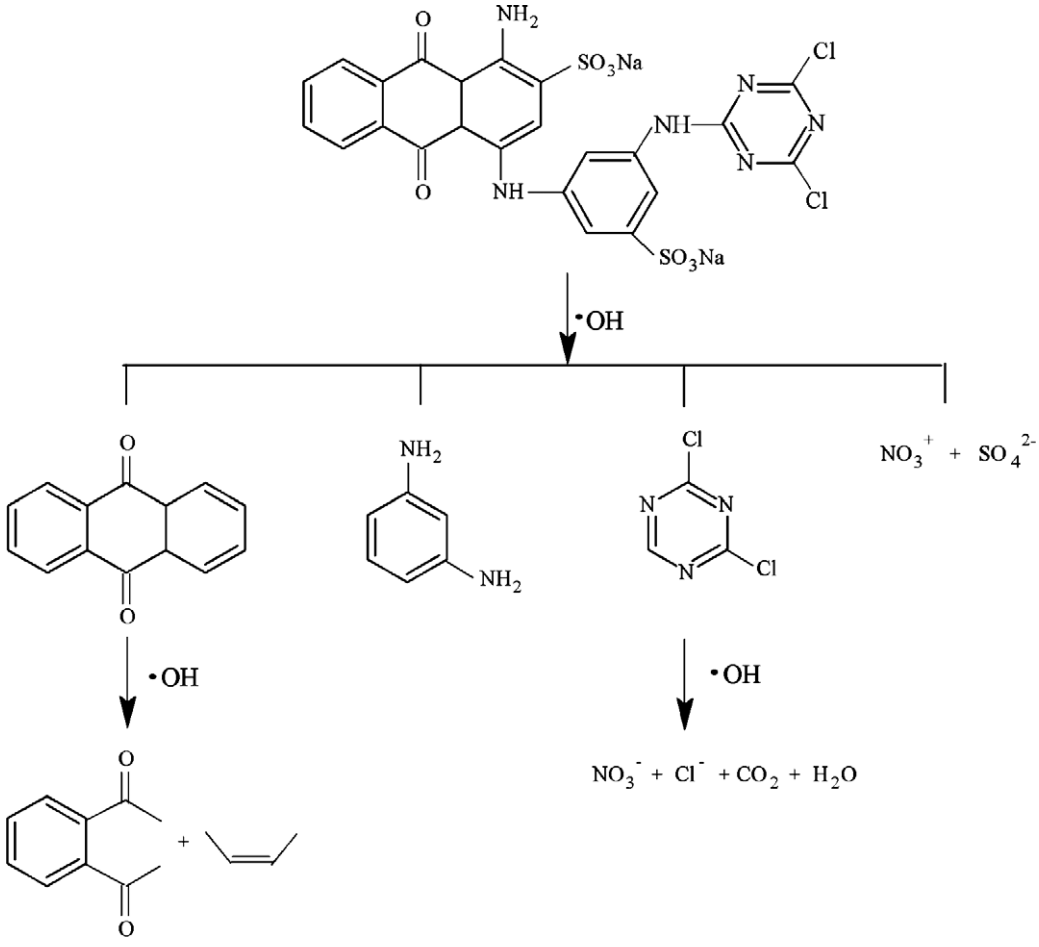

Fig. 4. Photocatalytic degradation scheme for CI. Reactive Blue 4 [51].

$$H^+ + O_2^{\cdot -} \rightarrow HO_2^{\cdot} \quad (15)$$

$$2HO_2^{\cdot} \rightarrow O_2 + H_2O_2 \quad (16)$$

$$O_2^{\cdot -} + e^- + 2H^+ \rightarrow H_2O_2 \quad (17)$$

$$H_2O_2 + e^- \rightarrow HO^{\cdot} + OH^- \quad (18)$$

$$Dye^{\cdot +} + (O_2^{\cdot -} \text{ or } HO_2^{\cdot} \text{ or } HO^{\cdot}) \rightarrow \text{intermediates} \rightarrow \text{finalproducts} \quad (19)$$

The reaction mechanism for the photocatalytic degradation of many organic dyes over ZnO particles has been extensively reviewed [24,49–51]. The number of intermediates in the reaction and ease of decomposition depend upon the nature of the organic dyes studied. The photocatalytic degradation of azo and anthraquinone groups is an interesting mechanistic example on the role of ·OH and $O_2^{\cdot -}$ radicals in ZnO-assisted heterogeneous photocatalysis of aromatic organic dyes. The mechanisms are presented in Figs. 4–6, respectively.

In the UV degradation of CI Reactive Blue 4 anthraquinone dye, several main intermediates have been reported over Nd-doped ZnO (Fig. 4) [51]. The results noticed that 1,3-phenylenediamine, 2,4-dichloride-1,3,5-triazine, 7,10-phenanthrenequinone and some inorganic ions such as NO_3^- and SO_4^{2-} were initially produced via the ·OH radical attack on the C–N and C–S bonds of CI Reactive Blue 4. With the further attack by the reactive radicals, the cleavage of phenyl rings in 7,10-phenanthrenequinone happened and rendered to the formation of 1,2-diacetylbenzene and butylene. Additionally, 2,4-dichloride-1,3,5-triazine was then oxidized through ring rupturing reactions to give final products of NO_3^-, Cl^-, CO_2 and H_2O.

Degradation of azo dyes has also been extensively studied [52–54]. Indeed, Methyl Red (MeRed) has been used as a model compound to test the photocatalytic efficiency of various catalysts. Comparelli et al. [54] proposed a reaction pathway for the ZnO photocatalytic degradation of MeRed in the presence UV irradiation (Fig. 5). Their findings showed that the first mechanism in the MeRed degradation involved the homolytic rupture of the bond between the amine nitrogen and methyl group by means of direct photolysis. This route was reported to occur consecutively leading to the formation of intermediates such as $C_{14}H_{13}N_3O_2$ and $C_{13}H_{11}N_3O_2$ (1 and 2, respectively). In the second mechanism, ·OH radicals attacked the aromatic rings of MeRed, in succession, mono- or di-hydroxylated intermediates such as $C_{14}H_{13}N_3O_3$, $C_{14}H_{13}N_3O_4$ and $C_{15}H_{15}N_3O_3$ (3–5, respectively) were generated. These aromatic intermediates were further oxidized through ring-opening reactions into low-molecular weight compounds, which led to the release of molecular nitrogen ultimately.

The solar degradation pathway of Reactive Red 120 (RR120) which is a more complex azo dye molecule was revealed by Velmurugan and Swaminathan [55] (Fig. 6). In the primary ZnO photocatalytic degradation processes, ·OH and/or $O_2^{\cdot -}$ radicals attacked the RR120 and yielded 2-[(2-hydroxyphenyl)diazenyl]-8-(1,3,5-triazin-2-ylamino)naphthalene-1,3,6-triol as an intermediate. Under the repetitive attack of ·OH and/or $O_2^{\cdot -}$ radicals, intermediates like 2,8-diaminonaphthalene-1,3,6-triol, 1,3,5-triazine-2,4-diamine, 2-aminobenzene-1,3-diol and naphthalene-1,2,6,8-tetrol were subsequently formed. Eventually, these aromatic intermediates were mineralized to NO_3^-, SO_4^{2-}, CO_2 and H_2O.

The kinetics of photocatalytic degradation of organic dyes usually follows the Langmuir–Hinshelwood (L–H) model [56,57].

$$r = -\frac{dC}{dt} = \frac{kKC}{1 + KC} \quad (20)$$

where r is the degradation rate of the reactant (mg/L min), C is the concentration of the reactant (mg/L), t is the irradiation time, k is the reaction rate constant (mg/L·min), K is the adsorption constant of the reactant (L/mg). At millimolar concentrations $C \ll 1$, the equation can be simplified to an apparent first-order equation:

$$\ln\left(\frac{C_o}{C}\right) = kKt = K_{app}t \quad (21)$$

or

$$C = C_o \exp(-k_{app}t) \quad (22)$$

where K_{app} is the apparent first-order rate constant given by the slope of the graph of ln C_o/C vs. t and C_o is the initial concentration of the reactant. Therefore, under the same condition, the initial degradation rate could be written in a form conforming to the apparent first-order rate law:

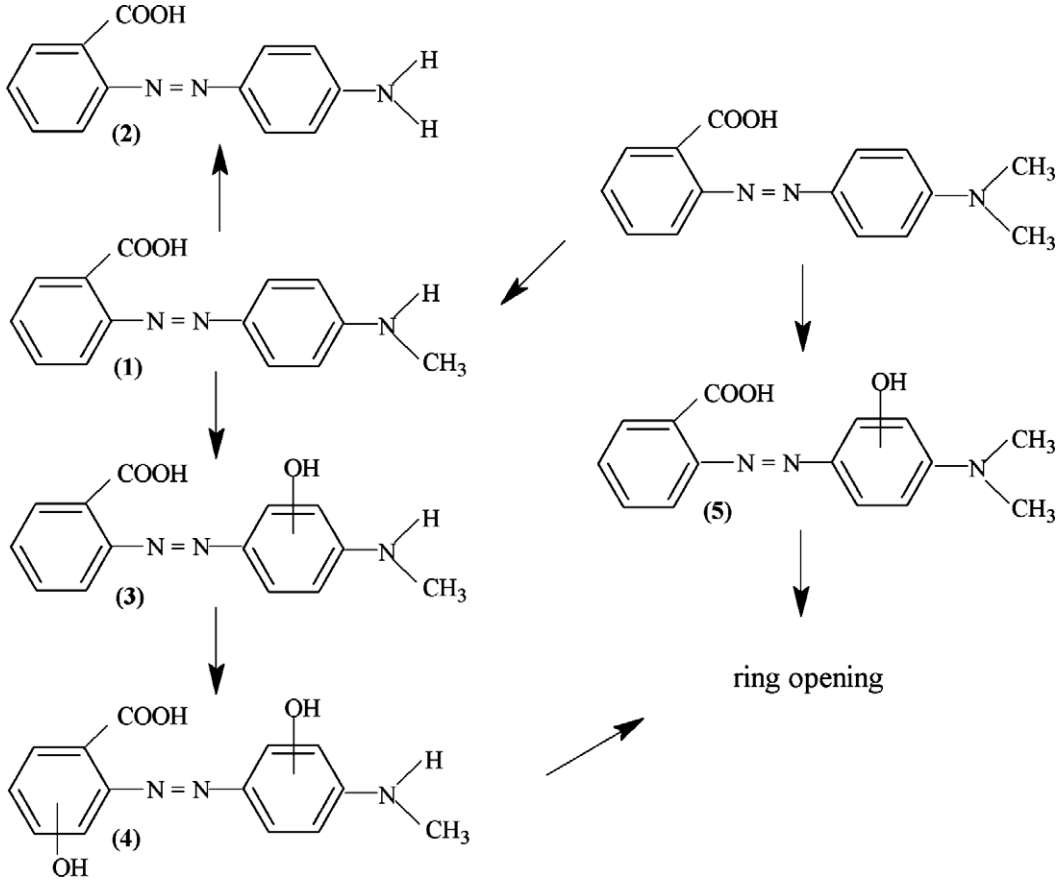

Fig. 5. Photocatalytic degradation scheme for Methyl Red [54].

$$r_0 = K_{app}C \quad (23)$$

First-order kinetic behaviour has been indicated in a number of instances in the organic dyes photocatalysis literatures [58–62]. At any rate, the L–H model serves as a basis for the photocatalytic degradation of organic dyes even if it could not directly give adequate fitting [63]. On the other hand, pseudo-zeroth order kinetic was also reported for suspended ZnO-assisted photocatalytic degradation of organic dyes [64].

3. Modification of ZnO

3.1. ZnO nanostructures

The degradation efficiency and rate of the catalyst are surface area dependent since electron–hole transfer takes place on the surface [65,66]. Thus, the catalyst morphology is an important property in determining the effectiveness of the catalyst. When the surface-to-volume ratio increases, the rate of electron–hole transfer from the semiconductor to the adsorbed molecule also increases due to the ability of the semiconductor to adsorb more molecules on its surface. There is also an added benefit that the rate of recombination of electron–hole pair decreases with an increase in the surface-to-volume ratio since the lifetime needed for the electron–hole pair to reach the surface from bulk is decreased and thus reducing the probability of recombination. For these reasons, many researchers have recently attempted and succeeded in creating a number of different morphologies of different sizes of ZnO such as nanopellets, nanorods, nanosheets, nanoflowers, nanoplates, nanopieces, nanoneedles, nanocups, nanocombs, nanowires and nanoplatelets [57,67–77]. Fig. 7 shows the morphologies of various ZnO nanostructures that have been reported in literature.

Warule et al. [73] developed sonochemical assisted hydrothermal method to prepare ZnO nanocups and nanoneedles for the degradation of Methylene Blue (MB) in the presence of UV light irradiation. The degradation efficiency of ZnO nanocups was shown to be slightly higher compared to ZnO nanoneedles due to the higher degree of crystallinity of the nanocups as

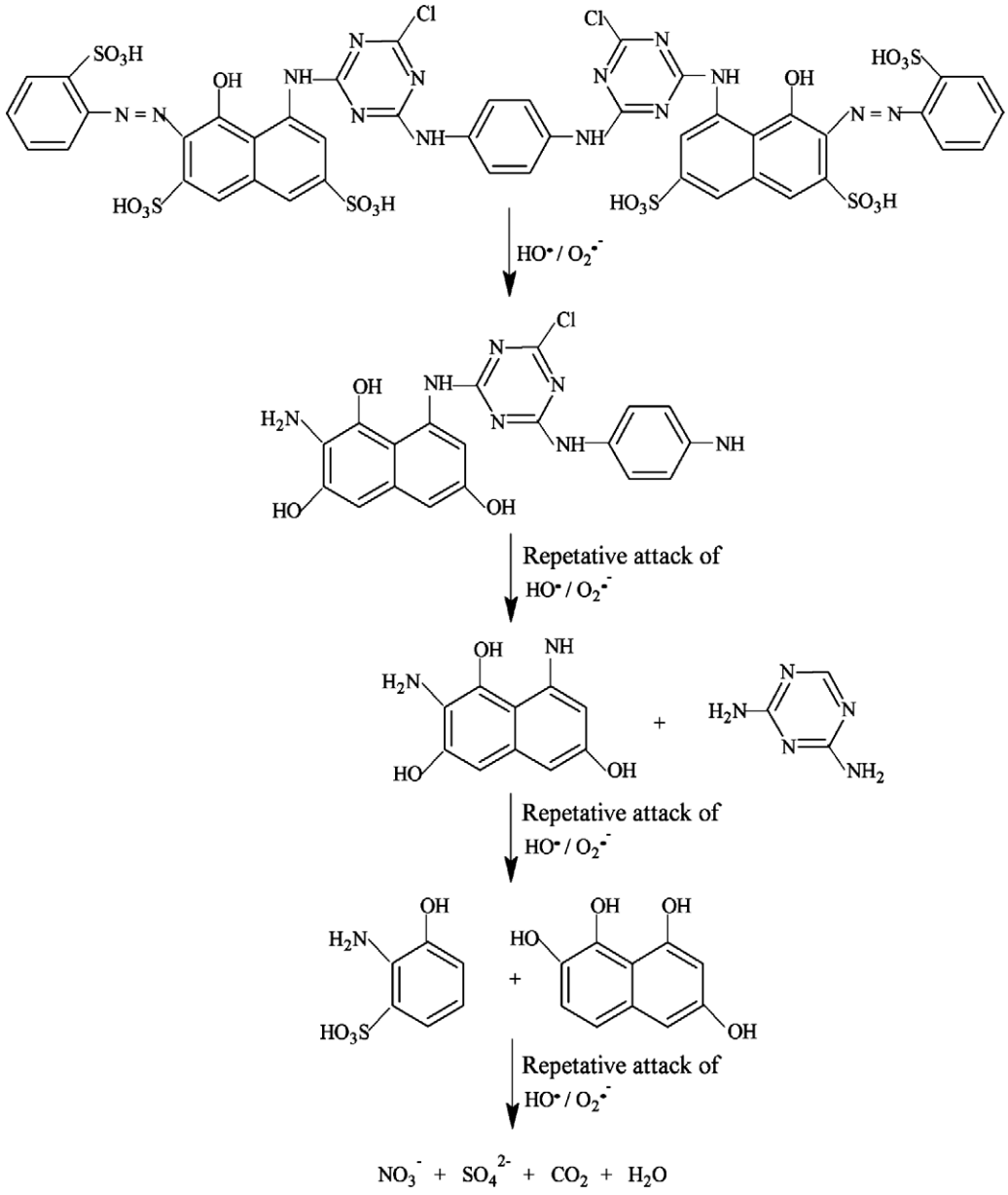

Fig. 6. Photocatalytic degradation scheme for Reactive Red 120 [55].

indicated in the XRD and TEM analyses. Under the experimental conditions, both of these nanostructures exhibited excellent degradation activities as compared to bulk ZnO and TiO_2-P25. This phenomenon was related to the nanocrystalline nature in which there was great enhancement in the activities as compared to bulk ZnO and TiO_2-P25. The degradation efficiencies of Methyl Orange (MO) over ZnO nanorods, nanoflowers and particles have also been used for comparison [78]. Their results showed that ZnO nanorods and nanoflowers were much superior to that of the ZnO particles. The difference in photocatalytic activity was attributed to their larger specific surface area and one-dimensional characteristic of the nanorods and nanoflowers. They also added that the higher the specific surface area was, the more oxygen molecules were adsorbed on the catalyst surface and the more ·OH radicals were produced for the dye degradation. Kansal et al. [79] compared the photocatalytic degradation of pararoaniline chloride dye over commercial ZnO and flower-like ZnO nanostructure. Their results showed that almost complete degradation of the dye was achieved in 18 min with synthesized ZnO whereas with commercial ZnO only 85% degradation was achieved in the same UV duration. The reason given by them was that the decrease in

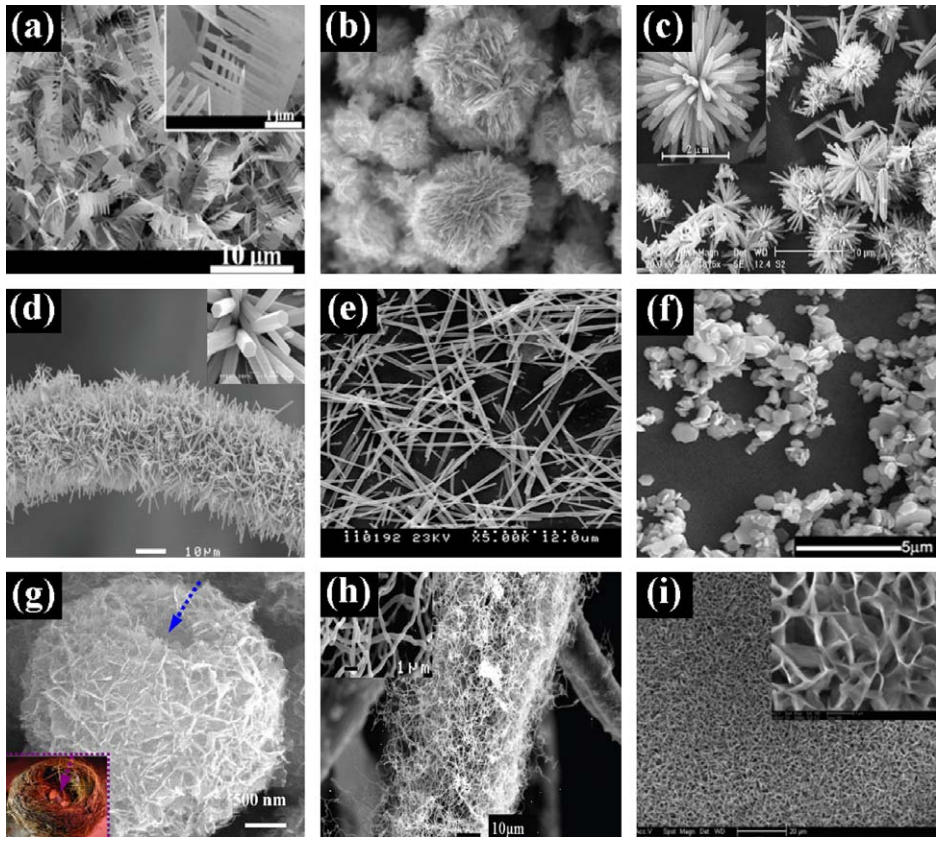

Fig. 7. ZnO nanostructure morphologies: (a) comb-like ZnO nanostructures [69], (b) ZnO balls made of fluffy nanosheets [74], (c) flower-like ZnO nanostructures [70], (d) ZnO nanorods grown on polyethylene fibers [75], (e) needle-like ZnO nanostructures [77], (f) plate-like ZnO [71], (g) nest-like hollow microsphere of ZnO nanopieces [72], (h) ZnO nanowires grown on polyethylene fibers [75] and (i) ZnO nanoplatelets [76].

crystallite size of the synthesized ZnO increased its surface area and thereby increasing the available average active sites for the dye degradation. The decrease in crystallite size also resulted in higher photo-ionic efficiency from a higher interfacial charge carrier transfer rate.

Zhu et al. [72] tested the photocatalytic degradation of Methyl Orange (MO) through hydrothermal synthesized mesoporous ZnO nanopieces-based nest-like hollow sphere and commercial ZnO powders. Under UV light irradiation, the photocatalytic degradation efficiencies were reported to be higher in hydrothermal synthesized ZnO nanopieces-based microsphere compared to that of ZnO powders. This was related to the mesopore in the ZnO nanopieces and specific micro-nanostructure constructed by the adjacent nanopiece led to high surface area and high utilizing efficiency of the UV light. Using ZnO nanostructures in the shape of particle, rod, flower-like and microsphere synthesized by hydrothermal method, the effect of morphology on the photocatalytic degradation of CI Acid Red 27 (AR27) solution has been investigated under sunlight irradiation [70]. XRD patterns showed that all the synthesized ZnO nanostructures have hexagonal wurtzite structure with high crystallinity and crystallite sizes in the range of 67–100 nm. UV–visible (UV–vis) absorption spectra indicated that the ZnO nanorods have higher visible light harvesting as compared to the other morphologies. The degradation obeyed the first-order kinetic rate with the kinetic constants of $4.5–19.5 \times 10^{-3}\,\mathrm{min}^{-1}$ dependent on the ZnO morphology and surface area. Chen and Lo [80] studied the photocatalytic degradation of Methyl Orange (MO) using different ZnO catalysts in the presence of UV light irradiation. In comparison to commercial ZnO powder, microwave synthesized ZnO nanotube was reported to have a better photocatalytic activity. This enhancement was due to the fact that the synthesized ZnO with hollow tubular structure has a surface area of $380.4\,\mathrm{m}^2/\mathrm{g}$ that was hundreds times larger than ZnO powder with a surface area of $5.2\,\mathrm{m}^2/\mathrm{g}$.

Umar et al. [74] studied the photocatalytic degradation of MB using ZnO balls made of fluffy thin nanosheets prepared by low-temperature solution process. FESEM and TEM analyses indicated that the

synthesized ZnO were made by accumulation of hundreds of thin ZnO nanosheets arranged in ball-like morphologies. XRD analysis showed that of as-synthesized ZnO were well crystalline and possessing wurtzite hexagonal phase. UV–vis absorption revealed that good optical properties for as-synthesized ZnO balls. Under UV light irradiation, the degradation of MB was shown to be almost completed in the presence of ZnO balls composed of nanosheets within 70 min. In addition, the synthesized ZnO balls were reported to exhibit superior photocatalytic performance as compared to TiO_2–UV-100 catalyst. Ye et al. [76] compared the efficiency of ZnO nanoplatelet synthesized by aqueous solution growth method with ZnO nanorod for the degradation of Eosin B, Methyl Orange and MeRed. The ZnO nanoplatelet was reported to show higher photocatalytic efficiency in degrading of all the organic dyes than ZnO nanorod. Under the experimental conditions, the degradation of Eosin B by ZnO nanoplatelet was also significantly higher compared to ZnS nanoparticle and Degussa P25 TiO_2. The higher activity of ZnO nanoplatelet was attributed to the larger surface area and unique nanostructure in this synthesized catalyst. Yan et al. [57] considered the photocatalytic activities of different catalysts including ZnO nanoneedles, nanoparticles, TiO_2 films and flower-like ZnO nano/microstructures for the degradation of MB. After 3 h UV irradiation, the degradation efficiency of MB was shown to follow ZnO nanoneedles > nanoparticles > TiO_2 films > flower-like ZnO nano/microstructures. The observed variation in the efficiency was related to the higher separation efficiency of electron–hole pairs in the ZnO nanostructures with high crystallinity synthesized by thermal evaporation.

3.2. Semiconductor coupling

The major limiting factor in the application of ZnO in the degradation of organic dyes in water is the high rate of recombination of the photogenerated electron–hole pairs. This leads to the poor rate of electrons and holes reaching the interface between semiconductor and water, where the degradation is inherent to occur. This problem can be addressed by coupling of two semiconductors possessing suitable energy levels for their corresponding conduction and valence bands. The coupling of a large band gap semiconductor with a small band gap semiconductor of a more negative CB level can result in the injection of e_{cb}^- from the small band gap semiconductor to the large band gap semiconductor, which is helpful for electron–hole separation (Fig. 8) [81]. Besides strengthening charge separation by isolating electrons and holes in two distinct

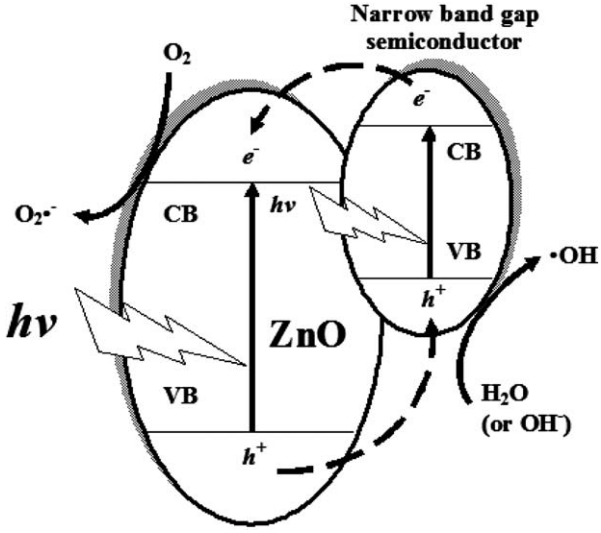

Fig. 8. The charge transfer process between ZnO and semiconductor with a narrow band gap.

semiconductors, it also allows the extension of the absorption threshold of light to a lower energy level. Therefore, the use of composite semiconductors for organic dyes degradation is feasible under visible light illumination.

Sathishkumar et al. [82] investigated the photocatalytic activity of CuO/ZnO nanocomposites prepared by impregnation method for the degradation of Acid Red 88 (AR88) under visible light irradiation. Their results showed that the combination of two semiconductors exhibited better photocatalytic activity and almost two-fold greater than that of pure ZnO at the same concentration. Such high efficiency reported by them was due to effective electron–hole transfer capability of CuO narrow band gap semiconductor to ZnO semiconductor. They added that the CB electrons of CuO were injected to ZnO CB, while the ZnO valence band holes were injected to CuO valence band during the visible light irradiation. Moreover, the optical absorption spectra analysis revealed that CuO/ZnO could absorb photons with wavelength in the range of 550–800 nm. Wei et al. [83] compared the photocatalytic degradation of Methyl Orange using ZnO film and CdS/ZnO film coated onto indium tin oxide (ITO) glass substrates through electrodeposition method. Their results also showed that ITO/CdS/ZnO film exhibited a higher photocatalytic activity than pure ZnO film. This enhanced effect was due to the charge transfer occurred between the interface of the composite film. The effective injection of electrons from CdS into ZnO can be further transported to the adsorbed molecular oxygen to form active $O_2^{\bullet-}$ radicals, which played a role in the enhancing of photocatalytic activity of ITO/CdS/ZnO film. The study of

Saravanan et al. [84] also showed that the degradation of MB using coupled CdO with ZnO nanorods was better than those of pure ZnO in the presence of visible light irradiation. UV–vis absorption studies indicated that the light absorption wavelength of CdO/ZnO extended into the red region as compared to pure ZnO which was in the blue region. The band gap energy of the composite was estimated as 2.99 and 3.20 eV for pure ZnO. They went further to ascribe that this enhancement was related to better light absorption and efficient charge transfer. Yan et al. [85] studied the photocatalytic degradation of Methyl Orange (MO) using α-Fe_2O_3/ZnO prepared by microwave hydrothermal synthesis. The degradation of dye solution was reported to increase by more than 3.5 times as compared to in a neat catalyst under UV light irradiation. This improvement was attributed to the formation of α-Fe_2O_3/ZnO heterojunction resulting in the charge transferring between the photoexcited α-Fe_2O_3 and ZnO.

Besides coupling with small band gap semiconductors, ZnO coupled with large band gap semiconductors such as SnO_2, ZnS, CeO_2, TiO_2, MoO_3 and WO_3 have also been investigated and proven to be efficient for the organic dyes degradation [86–91]. Wang et al. [86] studied the photocatalytic degradation of Methyl Orange (MO) using SnO_2/ZnO prepared by co-precipitation method. Under UV light irradiation, coupling of 33.3 mol% of SnO_2 with ZnO was more effective than ZnO and SnO_2 used separately. As the CB of ZnO was more negative than that of SnO_2, the latter served as a sink for the photogenerated electron in the coupled oxides. On the other hand, the photogenerated hole in SnO_2 was reported to transfer to the valence band of ZnO, making charge separation more efficient and thus the recombination of electron–hole in SnO_2/ZnO was greatly suppressed. Wang et al. [92] prepared TiO_2 nanotube/ZnO coupled with ZnO percentage (wt%) ranging from 10 to 30 wt% through a facile chemical method at room temperature. The photocatalytic efficiency of the TiO_2 nanotube/ZnO composite on Rhodamine B (RhB) degradation was strongly dependent on the proportion of ZnO in coupled catalysts. Under UV light irradiation, the degradation rate of TiO_2 nanotube/ZnO coupled with ZnO proportion of 20 wt% was superior to that of P25, ZnO and TiO_2 nanotube. They suggested that the increased photocatalytic activity of the TiO_2 nanotube/ZnO was ascribed to the enhanced charge separation derived from the coupling of TiO_2 with ZnO, which would promote interfacial charge transfer relative to that of charge-carrier recombination. The influence of WO_3/ZnO composite with different WO_3 concentrations from 1 to 8 wt% on the photocatalytic degradation of Acid Orange II has also been investigated [91]. Fourier-transform infrared (FTIR) analysis indicated the presence of more –OH groups and the formation of W–O–Zn bond in the synthesized WO_3/ZnO. The UV-DRS analysis showed that the addition of WO_3 into the composite caused the light absorption to shift towards longer wavelengths, which was reported due to the formation of the energy level of vacancy oxygen as when W^{6+} was doped into the crystal lattice of ZnO. Their UV photocatalytic results showed that all WO_3/ZnO composites exhibited higher Acid Orange II degradation than that for the similar system with ZnO alone. The rate constant of the catalyst increased with increase in the WO_3 concentration up to 2 wt.% and then decreased. The photocatalytic activity enhancement due to the prepared composite was related to the better separation of photogenerated charge carriers as shown in their PL emission spectra. A CeO_2/ZnO composite nanofiber was fabricated via the electrospinning technique by Li et al. [88]. RhB was quickly degraded about 98% in 3-h UV irradiation using CeO_2/ZnO composite nanofiber. While with the same reaction time, the RhB degradation efficiencies were only 17.4 and 82.3% for pure CeO_2 and pure ZnO nanofiber, respectively. This behaviour was ascribed to the formation of CeO_2/ZnO heterojunction. The electrons were reported to transfer from ZnO to CeO_2, while the holes were transferred from CeO_2 to ZnO. This can improve the separation photogenerated electrons and holes in the composites and thus enhanced the catalysing activity.

3.3. Metal doping

Modification of ZnO through metal ion doping is being considered widely for maximizing its photocatalytic efficiency. Doping with metal ion is regarded as one of possible way to shift the photo-response of ZnO into the visible region (Fig. 9a) [93]. In certain cases, the metal dopants can also act as electron/hole scavengers, leading to an increased lifetime of the charge carriers and by doing so reducing the probability of recombination processes [94] (Fig. 9b). This occurs through the following processes:

$$M^{n+} + e^-_{cb} \rightarrow M^{(n-1)+} \text{ (as electron trap)} \quad (24)$$

$$M^{n+} + h^+_{vb} \rightarrow M^{(n+1)+} \text{(as hole trap)} \quad (25)$$

If the $M^{n+}/M^{(n-1)+}$ pair is less negative than the ZnO CB edge and the energy level for $M^{n+}/M^{(n+1)+}$ is less positive than ZnO valence edge then the trapping of electrons and holes would happen on the surface,

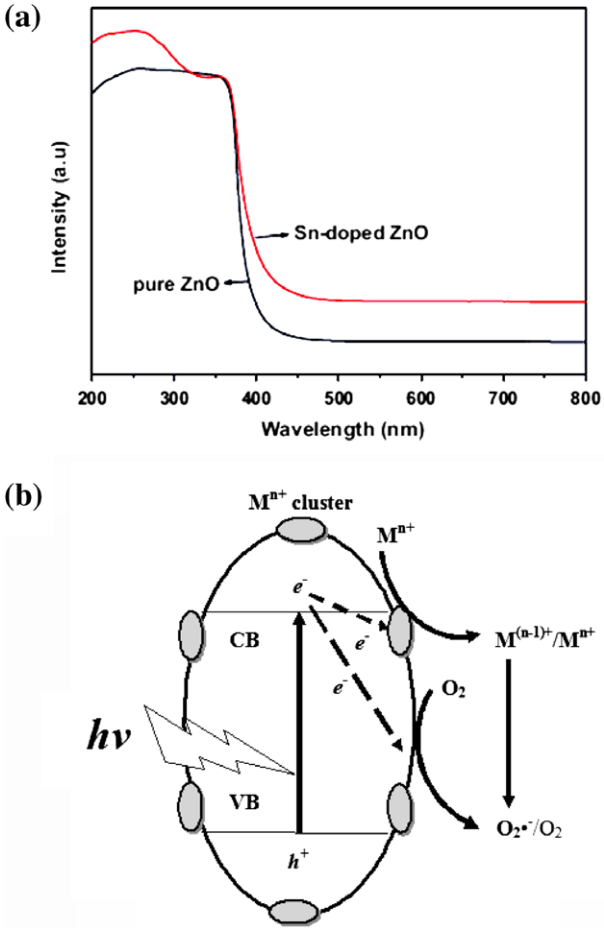

Fig. 9. (a) UV–vis spectra of Sn-doped ZnO [93] and (b) the excitation process in metal-doped ZnO.

affecting the lifetime of charge carriers. Successful metal ion doping near the surface of ZnO can result in enhanced efficiency of the photocatalytic system. Nevertheless, in literatures, negative photocatalytic results with metal ion doping have also been reported. The photocatalytic activity of metal-doped ZnO photocatalyst significantly depends on the selected metal ions and contents, preparation methods and operating conditions. In the case of deep doping, metal ions likely behave as recombination centers, as electron and/or hole transferring to the interface is more difficult. Moreover, there exists an optimum of doped metal ion concentration, above which the photocatalytic activity reduced due to the increase in electron–hole pair recombination [22,94].

It was found that Ag, Na, Fe, Co, Cr, Sn, La, Ta and V ions can increase the photocatalytic activity, while Mn, Cu and Pt ions caused detrimental effects. Different effects resulted from the different activities of various metal ions with regard to trapping and transferring electrons/holes. Sun et al. [93] examined the efficiency of Sn doping on the photocatalytic degradation of MB under solar irradiation. They found that Sn-doped ZnO has higher solar photocatalytic activity than pure ZnO on the MB degradation and mineralization. Under the experimental conditions, complete MB degradation was achieved after 6 h of irradiation and the corresponding COD and TOC removal was reported to be almost 100% after 10 h of irradiation. In contrast, the photocatalytic performances of pure ZnO were found to be 87% degradation, 48% COD removal and 71% TOC removal after 10 h of irradiation. The higher photocatalytic activity in the presence of Sn-doped ZnO was attributed to better dye adsorption and separation of photogenerated electron–hole pairs as evidenced in their N_2 adsorption and PL analyses. The UV photocatalytic activity of Ag-doped ZnO has also been studied by analysing the degradation of Orange G (OG) in aqueous solution [95]. In Ag-doped ZnO, the Ag content was varied from 0.35 to 2.90 at.%. The results in their report showed that undoped ZnO exhibited the lowest efficiency among all the tested catalysts. This indicated the importance of Ag doping for enhancing the photocatalytic performance of ZnO. The reported photocatalytic efficiency of OG increased in the order of ZnO < 0.35 at.% Ag-doped ZnO < 0.72 at.% Ag-doped ZnO < 2.90 at.% Ag-doped ZnO < 1.81 at.% Ag-doped ZnO. The deposition of Ag dopant on the surface of ZnO was reported to act as a sink for the electrons, to prolong the lifetime of the photogenerated charge carriers, to promote interfacial charge-transfer kinetics between the metal and the semiconductor and therefore improved the photocatalytic activity. Jia et al. [96] investigated the La-doped ZnO nanowires on the photocatalytic degradation of RhB by varying the doping concentration from 1 to 2.5 at.%. Pure ZnO gave a complete degradation of RhB in about 325 min of UV irradiation. On the contrary, 2.0 at.% La-doped ZnO degraded RhB completely from the solution within 200 min. The reason given by them was that when La^{3+} dissolved into ZnO, more surface defects could be produced and a space charge layer could be formed on the surface, which was beneficial to prevent the recombination of photogenerated electron–hole pairs.

Kong et al. [97] synthesized Ta-doped ZnO nanoparticle and analysed its photocatalytic activity under visible light. In their investigation, the influence of Ta doping content on the photocatalytic degradation of MB was examined. The Ta-doped ZnO samples were prepared by varying the doping content from 0.5 to 3.0 mol% of Ta. Their results revealed that the Ta doping in ZnO improved the activity of the photocatalyst significantly in comparison to pure ZnO. The Ta doping content was further tuned to achieve the optimum

photocatalytic activity and 1.0 mol% Ta-doped ZnO photocatalyst was reported to show the highest photocatalytic degradation of MB owing to the highest concentration of the surface hydroxyl groups and active defect sites as well as the largest specific surface area. Wu et al. [98] prepared Cr-doped ZnO nanowire and evaluated its photocatalytic activity using Methyl Orange (MO) as a model pollutant. After 140 min of visible light irradiation, MO solution can be obviously degraded by the Cr-doped ZnO. In contrast, MO degradation of pure ZnO took place at a much slower rate under the same conditions. The TOC results also showed that MO degradation greatly decreased in the presence of Cr-doped ZnO compared to pure ZnO. Zhou et al. [51] studied the effect of Nd^{3+} doping (1–3 mol%) on the photocatalytic degradation of CI Reactive Blue 4 under the dye concentration of 20 mg/L, stirred speed of 200 rpm and catalyst loading of 0.1 g/L. Their results showed that the degradation rate of Nd-doped ZnO was much higher when compared to that of pure ZnO. The rate constant of the catalyst increased with increase in the Nd loading up to 2.5 mol% and then decreased. The reason given by them was that the Nd^{3+} ion worked as an electron scavenger, which can react with the superoxide species and prevented the electron–hole recombination. An increase in Nd^{3+} ion concentration also caused higher surface barrier, narrower space charge region and hence the electron–hole pairs were efficiently separated by the large electric field.

Using Co^{2+} as dopant, Xu et al. [99] examined the photocatalytic degradation of Methyl Orange (MO) at different Co^{2+} doping concentrations from 0.5 to 5.0 mol%. XRD results showed that the ZnO powders were hexagonal wurtzite structures and their crystallization decreased with the increase of Co^{2+} doping concentration. Their SEM images displayed the morphology of catalysts were spherical which have a diameter of about 200 nm and UV-DRS spectra indicated that the absorption edge shifted to longer wavelength with the increase in the Co^{2+} concentration. Compared with undoped ZnO, the visible light photocatalytic activity of 3 mol % Co-doped ZnO was improved greatly. This was attributed to both better absorption in visible light region and the larger content of oxygen vacancies or defects produced by doping Co^{2+} ion. Wu and Huang [100] tested the photocatalytic degradation of Orange G (OG) using sol–gel synthesized Na-doped ZnO nanowires under UV irradiation. Their findings revealed that the photocatalytic activity of Na-doped ZnO increased gradually with increasing of the Na content (Na(1.2 mol%)-doped ZnO > Na(0.6 mol%)-doped ZnO > pure ZnO). However, when the Na content exceeded 1.2 mol% the photocatalytic activity of the catalyst decreased. Li et al. [101] studied the photocatalytic degradation of RhB using Au-doped ZnO hybrid nanoparticles. They observed that the RhB solution completely degraded by Au-doped ZnO within 10 min. On the other hand, pure ZnO took more than 20 min to obtain complete degradation of RhB. Slama et al. [102] studied the V-doped ZnO for the photocatalytic degradation of MB over the V content from 5 to 15 at.%. Under the conditions tested, optimal 10 at.% of V doping considerably improved the photocatalytic degradation of MB under visible light. The MB degradation was observed to follow a first-order kinetic model. The degradation rate constant was found to be $0.02599\,min^{-1}$ for 10 at.% V-doped ZnO compared to $0.01891\,min^{-1}$ for pure ZnO. This higher photocatalytic efficiency observed mainly for the V doping was attributed to the better performance of the absorption in visible range and increased content of oxygen vacancies.

On the contrary, Tsuzuki et al. [103] found that the photocatalytic degradation of RhB was impaired by Mn-doped ZnO. A continuous decrease in the degradation efficiency of the dye from 100% to about 70% as the dopant content increased from 0 to 5 at.% Mn was observed. They also found that the photocatalytic degradation of RhB was significantly slower in the presence of doped ZnO than undoped ZnO. Substitutional Mn^{3+} or Mn^{4+} in the interstitial position of ZnO was reported to act primarily as charge-carrier recombination center that shunted effective charge carriers away from the solid-solution interface with a net quenching in the photocatalytic activity [104,105]. Donkova et al. [104] examined the effect of Mn and Cu doping onto ZnO matrix on the photocatalytic degradation of MB dye under UV light. The degradation of MB was observed to be more favoured in the presence of undoped ZnO than in the presence of Mn-doped ZnO. The similar trend was also observed on their Cu-doped ZnO catalyst. They pointed out that certain of transition metals ZnO doping can at times be detrimental to the photocatalytic activities. The study of Pawinrat et al. [106] also showed that the degradation of MB dye using undoped ZnO was better than Pt-doped ZnO. The MB degradation efficiencies were found to be 54% for undoped ZnO compared to 50 and 55% for 1 and 3 wt.% of Pt-doped ZnO, respectively. The negative effect was attributed to the ohmic type of Pt which can facilitate discharge of the photogenerated electrons into the electrolyte. Thus, Pt-doped ZnO did not produce a longer electron–hole separation lifetime in accordance with their PL spectra measurements.

3.4. Non-metal doping

Over the last several years, the use of non-metal ions doping to enhance the photocatalytic activity of ZnO is increasing. Doping of non-metal ions such as carbon (C), nitrogen (N), fluorine (F) and iodine (I) in ZnO crystalline could increase the photocatalytic activities in the visible region, particularly in the solar irradiation. Unlike metal ions, non-metal ions less likely form recombination centers and thus they are more effective to improve the photocatalytic activity. Among the anion-doped ZnO, carbon doping has been claimed theoretically to have a potential advantage. This was due to the substitutional carbon in the ZnO matrix introduced new states (C 2p) near to the valence band edge of ZnO (O 2p) [107]. Accordingly, the valence band edge shifted to a higher energy than the pure ZnO and hence, narrowed the band gap. This type of band-gap narrowing was important if the C-doped ZnO catalyst was to give a positive response in the visible light region.

Liu et al. [108] tested the C-doped ZnO flowers for the photocatalytic degradation of RhB under the visible light irradiation ($\lambda \geqslant 420$ nm). They observed that C-doped ZnO flowers showed stronger absorption in the UV–vis range due to the carbon substitution at oxygen sites in the catalyst. The C-doped ZnO was reported to be efficient degradation of RhB and its photocatalytic activity was much better than commercial ZnO. In addition, the high photocatalytic activity of C-doped ZnO was attributed to the larger surface area of the doped catalyst, which could provide more active sites and photocatalytic reaction centers for the adsorption of pollutant molecules. Using Vitamin C as additive, Cho et al. [107] studied the effect of C doping onto the ZnO matrix for the photocatalytic degradation of Orange II. EDX, XPS and XRD analyses revealed that the substitution of oxygen with carbon and the formation of Zn–C bonds in the synthesized C-doped ZnO. UV-DRS analysis showed that C-doped ZnO has visible light absorption bands that were red-shifted relative to the UV exciton absorption of polycrystalline pure ZnO. Under the conditions examined, the degradation efficiency was shown to be 6.6 times higher compared to pure ZnO. This behaviour was ascribed to the carbon doping which shifted the light absorption to higher wavelength and thus efficiently increasing the photocatalytic activity in the visible light region.

The incorporation of N into ZnO also observed to substitute O sites. According to Li and Haneda [109], substitutional N-doping generated a new band close to the valence band of ZnO making a two-step transition to the CB in the presence of light irradiation. Chen et al. [110] studied the photocatalytic degradation of N-doped ZnO prepared by the decomposition of zinc nitrate in air for the degradation of 1.0×10^{-4} mol/L Methyl Orange (MO). Their results revealed that N-doped ZnO was shifted to a longer wavelength and its absorption intensity was also increased. The photocatalytic activity of N-doped ZnO was much higher than that of pure ZnO under visible light irradiation. This increase was related to the N-doped ZnO which has a narrower energy band gap and can be activated by visible light. Thus, more electrons and holes can be generated to take part in the photocatalytic degradation of MO.

In addition to C- and N-doping, the effect of F-doped ZnO has been studied. It was found that in F-doped ZnO the residual F atoms did not turn into ZnO to occupy O-atom sites to form Zn–F bonds. The presence of oxygen vacancies found in the ZnO led to two energy levels below the CB, which caused the defect-induced red shift in the F-doped ZnO [20]. Ahmad et al. [111] examined the photocatalytic activity of F-doped ZnO nanopowders synthesized by decomposing the F-doped ZnO_2 at 450°C for the degradation of MB under UV ($\lambda < 400$ nm) and visible light ($400\text{ nm} < \lambda < 800\text{ nm}$) irradiation. Their Raman analysis showed that the F-doped ZnO nanopowder has higher oxygen vacancies than the pure ZnO. Analysis of UV-DRS indicated that the doped ZnO has a strong emission in the visible range on photo excitation. The estimated band gap for F-doped ZnO using the Kubelka–Munk function was reported to be 3.0 eV which was much lower than the undoped catalyst. The reduction in band gap was attributed to the formation of a large number of defect levels below the CB upon F doping. As a consequence of higher oxygen vacancies, F-doped ZnO exhibited efficient photocatalytic activities under UV and visible irradiation for the degradation of MB dye solution.

Different from F-doped ZnO, I-doped ZnO showed narrower band gap and new absorption bands in the visible light region, which is similar to C- and N-doping as aforementioned. In the presence of UV and visible irradiation, Bouaifel et al. [112] investigated the photocatalytic degradation of RhB using hydrothermal synthesized I-doped ZnO nanoflowers deposited on glass substrate. Addition of iodic acid (5–20 vol.%) in the reaction mixture was reported to allow the introduction of iodine ions in the form of I^- or IO_3^- in the ZnO lattice as indicated by their XPS results. Indeed, the nanostructured ZnO films prepared in the presence of iodic acid displayed a large increase in visible luminescence, which reached a maximum at a concentration of 10 vol.%. Under UV light irradiation, both doped and undoped ZnO films showed comparable

activities. However, photocatalytic performance of I-doped ZnO films under visible light irradiation was significantly enhanced in comparison to that of undoped ZnO. This enhancement was related to the activation of a sub-band gap transition in I-doped ZnO nanostructured films.

4. Operational parameters on the degradation of organic dyes

4.1. Effect of initial dye concentration

Due to the fact that as the concentration of model pollutant increases, more and more molecules of the organic compound get adsorbed on the surface of the catalyst. The initial substrate concentration can influence the extent of photocatalytic reaction rate at the surface of the catalyst. Velmurugan and Swaminathan [55] investigated the effect of initial concentration on the photocatalytic degradation of Reactive Red 120 dye over ZnO nanoparticles under solar irradiation. Increase in the dye concentration from 1×10^{-4} to 4×10^{-4} M decreased the degradation rate k from 0.173 to 0.012 min^{-1}. Yang et al. [113] stated that the degradation efficiency of MB was strongly dependent on the initial dye concentration. The degradation efficiency of MB over the dumbbell-shaped ZnO photocatalyst synthesized by microwave method decreased from 100 to 72% with the increase of the MB concentration from 10 to 30 mg/L. Akyol and Bayramoğlu [114] studied the effect of initial concentration by varying from 50 to 200 mg/L on the photocatalytic degradation of Remazol Red RR. After 60 min of UV irradiation ($\lambda = 365$ nm), the dye degradation and TOC removal were found to decrease from about 100 to 60% and 80 to 10%, respectively with increasing initial dye concentration. Behnajady et al. [115] examined the effect of substrate concentration on the photocatalytic activity of immobilized ZnO film for CI. AR88 degradation under UV irradiation ($\lambda = 254$ nm). The results in their report noted that the AR88 degradation efficiency decreased with the increase in substrate concentration from 5 to 30 mg/L. This was due to the fact that the absorption of light by the dye solution at high concentration for a fixed amount of catalyst. Chakrabarti and Dutta [59] reported the effect of initial concentration on the photocatalytic degradation of MB and Eosin Y (EY) using ZnO nanoparticles. The degradation efficiency of MB decreased from 87 to 40% as the initial concentration increased from 25 to 100 mg/L. For the EY, the degradation efficiency was shown to decrease from 93 to 63% as the initial concentration of the solution increased from 25 to 50 mg/L, beyond which increase in the initial concentration the degradation efficiency did not affect the degradation significantly. The negative effect at a higher concentration was ascribed to the dye solution becoming more and more dense, which hindered the penetration of light to reach the catalyst surface and thus decreasing the absorption of photons by the catalyst. Pare et al. [26] examined the effect of initial concentration (1.0×10^{-5}–5.0×10^{-5} M) on the photocatalytic degradation of Acridine Orange (AO) containing 250 mg ZnO in the presence of visible light irradiation. The results showed that 90% of the initial concentration of AO was degraded after 150 min and complete degradation was observed within 180 min. The AO degradation was reported to follow a pseudo first-order kinetic. The observed rate constant was found to vary from 0.0277 to 0.0051 min^{-1} as the initial concentration increased. When the dye concentrations are high, a greater number of dye molecules are adsorbed virtually on the ZnO surface. On the contrary, the relative number of oxidative species such as $^{\cdot}OH$ and $O_2^{\cdot-}$ radicals attacking the dye molecules decreased due to other operating conditions that are constant. Sobana and Swaminathan [60] investigated the effect of initial Direct Blue 53 (DB53) concentration over the concentration range of 1×10^{-4} to 9×10^{-4} M using ZnO physically mixed with activated carbon (AC–ZnO) under solar irradiation. At the concentration of 1×10^{-4} M, DB53 was totally degraded within 60 min. The degradation of DB53 followed a pseudo first-order kinetic and the observed rate constant was varied from 8.35×10^{-2} to 0.35×10^{-2} min^{-1} as the concentration increased from 1×10^{-4} to 9×10^{-4} M. As shown in many literature reports, the initial substrate concentration dependence of the degradation rate of dye can be realized by the fact that the photocatalytic reaction occurs on ZnO particles as well as in solution. On the surface of ZnO particles, the reaction occurs between the $^{\cdot}OH$ radicals generated at the active OH^- sites and dye molecules from the solution. When the initial substrate concentration is high, the number of these available active sites is reduced by dye molecules because of their competitive adsorption onto ZnO surface. Since the intensity of light and irradiation time are constant, the $^{\cdot}OH$ radicals formed on the surface of ZnO remained practically the same. Thus, the active $^{\cdot}OH$ radicals attacking the organic pollutants decreased due to the lower ratio of the $^{\cdot}OH$/dye. In addition, a significant amount of light may also be absorbed by the dye molecules rather than the ZnO at a higher initial substrate concentration. This condition can be ascribed to the increase in the initial concentration which led to less photons reaching the ZnO surface and resulted in a slower production of $^{\cdot}OH$ radicals. Consequently, the

degradation rate is decreased, since fewer ·OH radicals are available to degrade more dye molecules. Furthermore, the formation of intermediates during the photocatalytic reaction of target pollutant also affected the reaction rate. The generated intermediates may compete with the dye molecules for the limited adsorption and active sites on the ZnO surface. According to several authors [116–119], this competition could be more marked in the presence of a high concentration level of reaction intermediates produced by the degradation of higher initial dye concentration.

4.2. Effect of organic dye kinds

Wang et al. [120] investigated the photocatalytic activities of various organic dyes with different molecular structures and chemical compositions in the presence of Er^{3+}-doped $YAlO_3/ZnO/TiO_2$ composites. Under solar light irradiation, the reported pattern of photocatalytic degradation of Methyl Orange (MO), RhB, Azo Fuchsine (AF), Methyl Blue (MB) and Congo Red (CR) dyes ($C_o = 10$ mg/L) followed in the order of MB > CR > AF > RhB > MO. The observed variation in the degradation ratios of different dyes was related to their adsorption ratios. They went further to describe that different dye molecules have different charges after ionization, indicating the electrostatic attraction or repulsion have occurred between different organic molecules and catalyst particles, which resulted in the different adsorption and degradation ratios. Using ZnO as catalyst, Chakrabarti and Dutta [59] compared the photocatalytic activities of MB and EY that differed in their molecular structure and functional group. Under the conditions tested, the degradation efficiencies after 2 h UV light irradiation were found to be 58% for MB compared to 39% for EY. On the contrary, the removal of COD for MB was reported to be 24%, whereas that for EY was only 8.1%. The difference in photocatalytic activities was related to the variation in adsorption behaviour. Using Pt-doped ZnO coated on glass as catalyst, the photocatalytic degradation activities of different classes of dyes were shown to be in the following order: CI. Reactive yellow 84 (RY 84) > Eriochrome Blue Black B (EBB) > CI Reactive Red 195 (RR 195) > Methyl Orange (MO) [121]. The influence of the molecular structure on the photocatalytic degradation of MeRed and Methyl Orange (MO) has also been investigated over ZnO [54]. Their results reported that the degradation efficiency of MeRed was higher than that of MO after 145 min of UV light irradiation. The variation in the photoreactivity of MeRed was ascribed to the presence of –COOH group in ortho position with respect to the azo bond could increase the susceptibility attack of ·OH radicals due to positive electronic effects. They also added that loss of planarity of the MeRed molecule, sterically induced by the proximity between the –COOH and the azo bond may reduce the N=N π overlap, which in turn benefits the dye reactivity toward ·OH radicals. Tong et al. [122] studied the photocatalytic degradation of Rhodamine 6G (Rh 6G), RhB and Erythrosine B (Er B) over ZnO hierarchical nanostructures. Their results showed that all the dyes' degradation followed the pseudo first-order reaction in the presence of UV light irradiation. The observed apparent rate constants were found to be 0.899, 0.885 and 0.299 h^{-1} for Rh 6G, RhB and Er B, respectively. The photocatalytic activities of the resulting ZnO for Rh 6G and RhB were higher than those for Er B, which were related to their different absorption abilities onto the hierarchically nanostructured surface. Sun et al. [123] compared the photocatalytic activities of dumbbell-shaped ZnO on the degradation of Crystal Violet (CV), Methyl Violet (MV) and MB. The photocatalytic degradation of the tested compounds was reported in the following order of MB > MV > CV. This was attributed to the variation in adsorption behaviour due to different chemical structures.

4.3. Effect of catalyst loading

It is well documented that the photocatalytic degradation rate and efficiency would increase with catalyst loading. The increase in the efficiency seems to be due to the effective surface of catalyst area and the absorption of light. At lower catalyst loading, the absorption of light controlled the photocatalytic process due to the limited catalyst surface area. However, as the catalyst loading increased, an increase in the active sites of ZnO is obtained. The enlarged amount of photons absorbed and the amount of dyes adsorbed on the ZnO surface improved the photocatalytic degradation. When the ZnO loading is overloaded, nevertheless, owing to an increase in the particles aggregation, the surface that absorbed the photons is not increasing in a geometrical ratio [124]. In addition, the number of active sites on the ZnO surface also decreased because of the decrease in light penetration due to light scattering effect with an increase in the turbidity of the suspension and leading to the shrinking of the effective photoactivated volume of suspension. The integration of these two reasons resulted in a reduced performance of photocatalytic activity rather than the linearly increase with the overloaded catalyst. Hence, many researchers have verified that there was an optimum amount of catalyst loading in

Table 2
Effect of catalyst loading on the photocatalytic degradation of various dyes.

Dye degraded	Concentration (mg/L)	Irradiation/ time	Photocatalyst	Tested catalyst concentration (g/L)	Optimum catalyst concentration (g/L)	Degradation/ mineralization efficiency	References
Acid dye							
Acid Violet 7	283	30 min UV irradiation	ZnO	1.0–5.0	2.0	0.0388 min^{-1}	Krishnakumar and Swaminathan [129]
Eosin Y	50	120 min UV irradiation	ZnO	0.5–5.0	2.5	74% 49%[a]	Chakrabarti and Dutta [59]
Acid Brown 14	311	180 min solar irradiation	ZnO	0.5–3.0	2.5	2.48×10^4 s^{-1}	Sakthivel et al. [23]
C.I. Acid Yellow 23	40	60 min UV irradiation	ZnO	0.15–0.9	0.75	93%	Behnajady et al. [130]
Acid Red B	10	30 min solar irradiation	Er^{3+}-doped $YAlO_3$/ZnO	0.25–1.25	1.0	~85%	Wang et al. [131]
C.I. Acid Orange 7	20	60 min UV irradiation	ZnO	0.1–0.2	0.16	~98%	Daneshvar et al. [132]
Methyl Orange	10	120 min UV irradiation	ZnO	0.4–5	2.5	~95%	Chen et al. [133]
Acid Red 1	100	80 min UV irradiation	ZnO	0.1–2.0	0.5	100%	Hameed et al. [6]
Basic dye							
Basic Blue 11	50	1440 min visible irradiation	ZnO	0.25–1.0	0.5	~98%	Lu et al. [49]
Rhodamine B	23	180 min solar irradiation	ZnO	1.0–8.0	6.0	~0.045 min^{-1}	Byrappa et al. [134]
Methylene Blue	50	120 min UV irradiation	ZnO	1.0–10.0	6.0	76% 32%[a]	Chakrabarti and Dutta [59]
Acridine Orange	5	180 min visible irradiation	ZnO	2.0–7.0	5.0	0.0234 min^{-1}	Pare et al. [26]
Ethyl Violet	50	360 min UV irradiation	ZnO	0.1–2.0	1.0	1.4 h^{-1}	Chen [24]
Direct dye							
Direct Yellow 12	34	70 min UV irradiation	ZnO	1.0–5.0	4.0	1.1 μM min^{-1}	Rao et al. [135]
Congo Red	75	120 min solar irradiation	ZnO	0.025–0.25	0.16	97%	Annadurai et al. [136]
Direct Blue 53	288	60 min solar irradiation	ZnO/AC	1.0–6.0	5.0	0.0519 min^{-1}	Sobana and Swaminathan [60]
Mordant dye							
Alizarin Yellow GG	100	40 min UV irradiation	ZnO	1.0–4.0	3.0	0.070 min^{-1}	Hayat et al. [137]
Reactive dye							
Reactive Red 120	260	30 min solar irradation	ZnO	2.0–6.0	4.0	0.048 min^{-1}	Velmurugan and Swaminathan [55]
Remazol Red F3B	150	60 min UV irradiation	ZnO	0.5–2.5	2.0	~100% 53%[b]	Akyol and Bayramoğlu [114]
Procion Blue HERD	25	75 min UV irradiation	ZnO	0.5–2.0	1.0	100%	Bansal and Sud [138]
Reactive Blue 4	200	120 min UV irradiation	ZnO/Sepiolite	0.1–0.5	0.5	100%	Xu et al. [139]
Reactive Black 5	496	60 min UV irradiation	ZnO	0.5–4.0	2.0	~85%	Amisha et al. [140]
	496	60 min solar irradiation	ZnO	0.5–4.0	3.0	~60%	Amisha et al. [140]

[a]COD removal.
[b]TOC removal.

the photocatalysis studies [63,125–128]. Table 2 lists the effect of catalyst loading on the photocatalytic degradation of various dyes in numerous studies. Lu et al. [49] studied the effect of ZnO concentration (0.25–1.0 g/L) on the photocatalytic degradation of Basic Blue 11 (BB-11) irradiated using visible lamps. The photocatalytic degradation rate of BB-11 was found to increase and then decreased with the increase in catalyst concentration. The optimum concentration of ZnO was reported to be 0.5 g/L. The observed low degradation rate of BB-11 at high catalyst concentration was due to aggregation of ZnO particles and scattering light effect. Velmurugan and Swamninathan [55] noted that the degradation rate constant of Reactive Red 120 increased from 0.029 to 0.048 min^{-1} as the concentration of ZnO increased from 2 to 4 g/L in the presence of solar irradiation. However, increase in the catalyst loading from 4 to 6 g/L resulted in a decrease in the rate constant from 0.048 to 0.042 min^{-1}. Sakthivel et al. [23] carried out a series of experiments to assess the optimum ZnO catalyst loading by varying the amount of catalyst from 0.5 to 3.0 g/L in the Acid Brown 14 dye solution (dye concentration = 5×10^{-4} mol/L, pH = 9.93). Under solar irradiation, the rate of dye degradation increased linearly from 0.88×10^4 to 2.48×10^4 s^{-1} with catalyst loading up to 2.5 g/L. Above this loading, increase in turbidity of the solution reduced the light transmission through the solution. While below this level, they ascribed that the catalyst surface and absorption of light by ZnO were the limiting factors.

Under the experimental conditions (initial dye concentration = 7.31 mg/L, pH = 7.7, light intensity = 19.8 W/m), Nishio et al. [32] examined the effect of catalyst loading on the photocatalytic degradation of Orange II using ZnO as catalyst. The degradation rate constant, k increased rapidly with the increase in ZnO loading up to 1,000 mg/L. At higher loadings beyond 1,500 mg/L, however, they observed that the rate constant reached a constant value and suggested an optimal level for catalyst effectiveness existed. Using the AR88 as the model pollutant, Behnajady et al. [141] studied their photocatalytic activities using Ag-doped ZnO with different catalyst dosages ranging from 100 to 600 mg/L. They also found that the degradation efficiency was improved until a certain limit of catalyst dosage and then further increase led to the adverse effect. The optimum ZnO loading was reported to be 400 mg/L for efficient degradation of AR88. The photocatalytic degradation was related to the formation of ·OH and $O_2^{\cdot-}$ radicals, which are the critical oxidizing species in the degradation process. Thus, the degradation efficiency of AR88 increased with the ZnO loading as the number of active species taking part for AR88 degradation increased as well. However, when the catalyst loading reached a certain limit, excess catalyst could cripple the transparence of solution and caused a scattering effect, which correspondingly reduced the light utilization rate and restrained the photocatalytic activity of ZnO. Byrappa et al. [134] studied the effect of catalyst loading on the photocatalytic degradation of RhB and observed an optimum catalyst concentration of 300 mg/50 mL in the dye solution for an efficient ZnO photocatalytic activity. At high catalyst concentration, the reported low degradation rate was attributed to the deactivation of activated molecules by collision with ground state molecules dominating the reaction. A consistent trend of results has been observed on the photocatalytic degradation of MB using ZnO calcined at 1,000°C [142]. The degradation efficiency was found to increase with increasing catalyst content up to a level of 0.25 mg/L and, on subsequent addition of catalyst from 0.25 to 1.00 mg/L led to level off the degradation efficiency. Wong et al. [131] tested the effect of catalyst loading on the photocatalytic degradation of Acid Red B using Er^{3+}-doped $YAlO_3$/ZnO composite in the range of 0.25–1.25 g/L. The optimum degradation was observed to be 1.0 g/L of prepared composite catalyst under the experimental conditions. An increase in the amount of catalyst below the optimum value provided greater number of available active sites for adsorption. In any given application, the optimum catalyst loading has to be determined in order to avoid an ineffective excess of catalyst and to ensure total absorption of efficient photons.

4.4. Effect of solution pH

The interpretation of solution pH effects on the efficiency of dye photocatalytic degradation process is a very difficult task because of its multiple roles [127]. Due to amphoteric behaviour of most semiconductor oxides, solution pH is a crucial parameter governing the degradation rate participating on semiconductor particle surface since it determines the surface-charge of the photocatalysts and size of aggregates formed. ZnO particle suspended in aqueous solution is also known to be amphoteric, the effect of solution pH on degradation rate depending on the acid-base properties of the semiconductor oxide surface and can be explained on the basis of zero point charge. The adsorption of water molecules on ZnO surface is followed by the dissociation of OH^- groups, leading to coverage with chemically equivalent metal hydroxyl groups as shown in the following acid-base equilibrium reactions:

$$Zn\text{–}OH_2^+ \leftrightarrow Zn\text{–}OH + H^+ \quad pK_{a1} \tag{26}$$

$$Zn\text{–}OH + OH^- \leftrightarrow ZnO^- + H_2O \quad pK_{a2} \tag{27}$$

where K_a is the acidity constant. The pK_a values for ZnO have been estimated as 7.6 for pK_{a1} and 11 for pK_{a2}, which resulted in a pH of zero point charge ($pH_{zpc} = 0.5(pK_{a1} + pK_{a2})$) of 9.3 [54]. Accordingly, ZnO surface is protonated below pH 9 and above this pH, catalyst surface is predominantly negatively charged by adsorbed OH^- ions. The presence of a large amount of OH^- ions on the ZnO surface as well as in the reaction solution favoured the formation of ·OH radicals, which are considered as principal oxidizing species responsible for degradation process at neutral or high pH levels and thus the efficiency of the process is logically enhanced. Although in some cases, it should be noted that in alkaline solution there is an electrostatic repulsion between the negatively charged surface of ZnO and the OH^- ions. This fact could hinder the formation of ·OH radicals and thus reduced the degradation rate [60,124]. Textile wastewaters usually containing a mixture of large complex organic pollutants may not be neutral. The dye pollutants present in wastewater differ greatly in several parameters, particularly in their speciation behaviour, solubility in water and hydrophobicity. While some dye pollutants exist in non-ionic forms at common pH conditions typical of natural water or wastewater, others exhibit a wide variation in speciation (or charge) and physico-chemical properties [143]. At a pH below its pK_a value, a dye pollutant is primarily in its molecular form. Above this pK_a value, a dye pollutant tends to undergo deprotonation becoming negatively charged. These characteristics can significantly affect the interaction and affinity between both photocatalyst and dye pollutant when a variation of solution pH takes place. Table 3 presents the pH influence on the photocatalytic degradation of various dyes.

Velmurugan and Swaminathan [55] studied the effect of pH in the range of 3–11 on the photocatalytic degradation of Reactive Red 120 (RR 120) over ZnO under solar light irradiation. The rate of degradation in acidic solution at pH 5 was found to be higher than the alkaline solution. The high degradation rate in the acidic solution was due to maximum adsorption of RR 120 onto the surface of positively charged ZnO nanocrystals. Fouad et al. [31] reported on the influence of pH on the photocatalytic degradation of CI. Reactive Black 5 (RB5, an anionic dye with sulphuric groups) over ZnO thin films under UV-A irradiation. Their results showed that the photocatalytic activity was most favoured at a lower pH (2.0) but went on at a slower and inefficient rate at pH 10.0. At low pH value, electrostatic interactions between the positively charged surface of ZnO and dye anions (which generated from the dissociation of sodium salt of the dye molecule, [dye-Na] → [dye^-] + [Na^+]) in aqueous solution lead to strong adsorption of the dye on the catalyst surface. Nevertheless, at high pH value, owing to RB5 has sulphuric groups in its structure was existed as negative charged anions and thus dye would not be adsorbed onto the surface of the ZnO effectively in alkaline solution. The study of Wang et al. [120] also showed that the degradation of Acid Red B dye under acidic conditions was better than in alkaline medium in the presence of Er^{3+}-doped $YAlO_3/ZnO/TiO_2$ composite. Precisely, after the solution was acidified from pH 11.0 to pH 3.0, a five-fold increase in degradation efficiency was obtained. Such an increase in degradation efficiency could be explained by the existence of two sulphonic groups in Acid Red B ionizied easily in acidic media and attracted to the positive surface of ZnO/TiO_2 particles. Using ZnO, Kansal et al. [33] studied the photocatalytic degradation of Reactive Black 5 (RB5) and Reactive Orange 4 (RO4) dyes at different solution pH values in the range of 3–11. The RB5 degradation was reported to be favourable in mild acidic solution due to Columbic attraction of the positively charged ZnO with the dye anions. However, RO4 was found to undergo degradation at faster efficiency at high pH value. It is important to note that the photocatalytic degradation of some dyes is more efficient in alkaline solution [148] and others at about neutral pH [30]. It has earlier been reported that in alkaline solution, there is a higher concentration of OH^- ions, which can lead to the photogeneration of more of the reactive ·OH radicals and thus increasing the efficiency of RO4 degradation. Wu [148] investigated the effect of pH on the photocatalytic degradation of C.I. Reactive Red 198 (RR198). After 120 min, irradiation, the degradation rate constants were 0.0116, 0.0534 and 0.0637 min^{-1} for UV/ZnO at pH 4, 7 and 10, respectively. Since the OH^- ions in alkaline solution acted as hole scavenger on the ZnO surface and produced ·OH radicals with strong oxidation power after they lost one electron. As a result, the probability of ·OH radicals formation was reported to be increased with pH and explained the high degradation rate of RR198 in alkaline solution with UV/ZnO system. Shahmoradi et al. [149] examined the effect of pH ranging from 2 to 12 on the

Table 3
Effect of solution pH on the photocatalytic degradation of various dyes

Dye degraded	Concentration (mg/L)	Irradiation/time	Photocatalyst	Range of solution pH	Optimum solution pH	Degradation/ mineralization efficiency	References
Acid dye							
Acid Red B	10	30 min solar irradiation	Er^{3+}-doped $YAlO_3$/ ZnO/TiO_2	3.0–11.0	3.0	100%	Wang et al. [120]
Acid Yellow 23	40	60 min UV irradiation	ZnO/SnO_2	2.28–9.52	8.05	~90%	Modirshahla et al. [35]
Acid Brown 14	311	180 min solar irradiation	ZnO	3.0–11.0	10	2.58×10^4 s^{-1}	Sakthivel et al. [23]
C.I. Acid Orange 7	20	60 min UV irradiation	ZnO	2.2–10.38	7.4	100%	Daneshvar et al. [132]
Biebrich Scarlet	25	20 min UV irradiation	ZnO	3.0–11.0	10.0	100%	Kansal et al. [144]
Acid Red 14	20	60 min UV irradiation	ZnO	4.0–12.0	7.0	100%	Daneshvar et al. [30]
Methyl Red	8	120 min UV irradiation	ZnO	2.0–12.0	6.0	~80%	Comparelli et al. [54]
Methyl Orange	10	120 min UV irradiation	ZnO	2.0–12.0	6.0	~60%	Comparelli et al. [54]
Basic dye							
Methylene Blue	10	120 min visible irradiation	Co-doped ZnO	4.5–12.5	12.5	0.0127 min^{-1}	Xiao et al. [145]
Acridine Orange	5	180 min visible irradiation	ZnO	2.9–7.1	7.1	0.0240 min^{-1}	Pare et al. [26]
Rhodamine B	5	100 min UV irradiation	ZnO	4.5–10.5	7.0	100%	Zhai et al. [146]
C.I. Basic Blue 41	20	60 min solar irradiation	TiO_2/ZnO	1.0–7.0	6.0	100%	Jiang et al. [89]
Methyl Green	50	1440 min visible irradiation	ZnO	4.0–10.0	10.0	100%	Mai et al. [50]
Direct dye							
Direct Yellow 12	34	70 min UV irradiation	ZnO	4.0–10.0	10.0	1.4 μM min^{-1}	Rao et al. [135]
Congo Red	5	12 min UV irradiation	ZnO	6.0–11.0	6.0	100%	Movahedi et al. [147]
Direct Blue 53	288	60 min solar irradiation	ZnO/AC	3.0–11.0	9.0	~100%	Sobana and Swaminathan [60]
Mordant dye							
Alizarin Yellow GG	100	40 min UV irradiation	ZnO	5.0–12.2	5.0	~80%	Hayat et al. [137]
Reactive dye							
Reactive Black 5	25	8 min UV irradiation	ZnO	3.0 –11.0	4.0	100%	Kansal et al. [33]
Reactive Orange 4	25	30 min UV irradiation	ZnO	3.0 –11.0	11.0	100%	Kansal et al. [33]
Remazol Red F3B	150	60 min UV irradiation	ZnO	6.0–10.0	7.0	~98% ~45%[a]	Akyol and Bayramoğlu [114]
CI Reactive Red 198	20	120 min UV irradiation	ZnO	4.0 –10.0	10.0	0.0637 min^{-1}	Wu [148]
Reactive Red 120	260	30 min solar irradiation	ZnO	3.0 –11.0	5.0	0.048 min^{-1}	Velmurugan and Swaminathan [55]
CI Reactive Blue 4	20	90 min UV irradiation	Nd-doped ZnO	3.0–13.0	11.0	91%	Zhou et al. [51]

[a]TOC removal.

photocatalytic degradation of Briliant Blue FCF (BBF) using ZnO modified with manganese. The maximum degradation efficiency was observed at extreme basic conditions due to the abundance of ·OH radicals or to the anionic form of the BBF dye to be oxidized compared to its molecular form. Using MB as dye pollutant, Kong et al. [61] tested the effect of pH ranging from 5 to 12 on the photocatalytic activity of Ta-doped ZnO. The degradation efficiency of MB was also higher in the alkaline condition with almost twofold enhancement as pH increased from 5 to 8. Further increase in pH from 8 to 12 affected the photocatalytic activity of the catalyst negatively. Thus at pH = 8, the maximum degradation efficiency was observed. Their findings revealed that the low degradation efficiency at low pH was due to the dissolution and photodissolution of ZnO. They also added that the increase of the degradation efficiency at alkaline pH was attributed to the high hydroxylation of the catalyst surface due to the presence of a large amount of OH^- ions. However, the electrostatic attraction was improved at higher pH, the hydroxyl groups decreased simultaneously. This led to the decline of the photocatalytic efficiency at pH > 8 due to the breakage of the hydroxylation on the catalyst surface. On the contrary, Daneshvar et al. [30] observed that the photocatalytic degradation of Acid Red 14 (AR14) dye using ZnO catalyst under neutral pH was beneficial and had higher degradation efficiency than in the alkaline medium. At acidic pH values, ZnO was reported to dissolve as Zn^{2+} and has no photocatalytic properties, while at basic pH values, it is transformed to negatively charged particles and repulsed the dye anion-molecules which originated from SO_3^- group substituted on the aromatic ring. Pare et al. [26] studied the effect of pH on the photocatalytic degradation of AO over ZnO using visible light irradiation. Their kinetic results indicated that the degradation rate increased when the solution pH increased from 3 to 7. Nevertheless, the degradation rate decreased at higher solution pH. The low degradation rates at acidic or at alkali pH values were due to dissolution and photodissolution of ZnO. At acidic pH, ZnO can react with acids to produce the corresponding salt, while at alkaline pH, it can react with a base to form complexes like $[Zn(OH)_4]^{2-}$. In summary, different dyes have different activities in photocatalytic reaction. Some are degraded effectively at lower pH, while others degraded effectively at higher pH. All these can be attributed to the nature of the pollutant to be degraded. Therefore, it is important to study the nature of the pollutants to be degraded and accurately determines the optimum solution pH for photocatalytic degradation of dyes.

4.5. Effect of light intensity and wavelength

Light irradiation plays a significantly important role in all of photocatalytic reactions and generates the photons required for the electron transfer from the valence band to the CB of a semiconductor photocatalyst. The energy of a photon is related to its wavelength and the overall energy input to the photocatalytic process is dependent on the light intensity. Therefore, the effects of both intensity and wavelength have been studied in numerous investigations for various organic pollutants including dyes. Earlier studies [63,150,151] on the effect of the light intensity have reviewed that at low light intensity (catalyst dependent, surface reaction limited) the rate is linearly proportional to the light intensity, while at medium-high intensity, the rate becomes proportional to the square root of the light intensity and at higher light intensity, the rate would not be affected by the increase in the light intensity. They have stated that this variation is due to the recombination of photogenerated electron and hole pairs under different irradiation intensities. Khataee and Zarei [152] investigated the effect of light wavelength using UV-A, UV-B and UV-C lights on the degradation of dye solution containing CI. Direct Yellow 12 (DY12) over immobilized ZnO. Under the experimental conditions (50 mg/L dye solution at pH = 3, UV-A (λ = 315–380 nm), UV-B (λ = 280–315 nm) and UV-C (λ = 100–280 nm) lights), the degradation efficiency of DY 12 after 90 min of irradiation was found in the following order of UV-C > UV-B > UV-A. The enhanced degradation efficiency with UV-C light irradiation was attributed to the fact that more ·OH radicals can be generated by photodissociation of the produced H_2O_2. Whereas, the UV-A and UV-B lights were reported to be unable to decompose the H_2O_2 to ·OH radicals. Akyol and Bayramoğlu [114] examined the influence of light intensity by varying nominal UV-A light power from 12 to 36 W on the photocatalytic degradation of Remazol Red F3B over ZnO catalyst. The degradation and TOC removal were observed to increase rapidly by increasing the light intensity up to 18 W and then the degradation and TOC removal increased gradually. They went further to describe their results were not linearly but power-law dependent on the light power and probably square root dependent, which indicated that the reactions were surface controlled to various extents. Sakthivel et al. [23] found that the solar degradation rate of Acid

Brown 14 increased linearly with increasing light intensity and its maximum value was in the range of 1.32×10^5–1.37×10^5 Lux. The results in their report suggested that sunlight energy was considered as low light intensity and thus the rate of dye degradation increased by increasing the light intensity. They added that sunlight was an energy source which contained 4.3% of UV (3.9% UV-A, 0.4% UV-B) and its intensity was calculated to be approximately 38.2 W/m^2. The effect of light intensity on the photocatalytic degradation of Remazol Red (RR) over ZnO was tested by turning on different numbers of UV lights ($\lambda = 254$ nm) from 2 to 6 corresponding to the light intensities of 0.53, 0.8, 1.06, 1.33 and 1.6 μeinstein/L s, respectively [153]. Their results also revealed that the degradation rate of RR increased with increasing the light intensity. Behnajady et al. [154] studied the effect of light intensity on the degradation of CI. AR27 using ZnO immobilized on glass plates under UV-C irradiation. Their results showed that the degradation efficiency increased steadily by increasing the light intensity linearly. The increase in the light intensity from 21.4 to 58.5 W/m^2 increased the degradation efficiency from 17.5 to 37.8%. The linear relation reported by them indicated that saturation of the catalyst by the incident photons was not reached and electron–hole pairs were consumed more rapidly by chemical reactions rather than by recombination. Shahmoradi et al. [148] carried out the photocatalytic degradation of Brilliant Blue FCF (BBF) in the presence of modified ZnO nanoparticles with manganese additives (2 and 5 mol %) under sunlight and UV irradiation ($\lambda = 264$ nm). The degradation efficiencies in the presence of modified ZnO nanoparticles with manganese additives (2 and 5 mol%) increased linearly along with the irradiation time and attained about 89.6% and 78.8%, respectively within 3.0 h of sunlight irradiation. In the case of UV irradiation, the degradation efficiencies were 61.5 and 55.6%, respectively. All the photocatalytic degradation results under sunlight and UV irradiation obeyed the pseudo first-order kinetics. Byrappa et al. [155] studied the effect of light intensity on the photocatalytic degradation of Acid Violet over ZnO/AC using different light sources. Sunlight (intensity = 8.425×10^{15} quanta/s), UV light (intensity = 2.3775×10^{15} quanta/s) and mercury vapour lamp, MVL (300 W, intensity = 3.31×10^{15} quanta/s) illumination were used. Solar irradiation was reported to be efficient for the degradation of Acid Violet and followed in the order of sunlight > UV > MVL. This effect was attributed to the higher energy illumination with sunlight than with UV and MVL lights.

4.6. Effect of co-occurring substances

Despite the fact that majority of the academic studies (as outlined in Tables 2 and 3 and also observed typically in the literature) concerned with the use of single-constituent model solution for the experiment works, the real wastewaters obtained from industries have a lot of organic and inorganic substances. Numerous studies have indicated that the co-occurring substances such as potassium, calcium, magnesium, copper, zinc, chloride, sulphate, nitrate, bicarbonate, carbonate and dissolved organic matters can influence the photocatalytic degradation rate of organic pollutants since they can be adsorbed onto the catalyst surface [89,156,157]. Depending on the chemical nature of the organic pollutants and solution pH in the photocatalytic system, they can also compete with organic pollutants for the available active sites of catalyst [130,157]. The competition for active sites involves the constant displacement of OH^- ions from catalyst surface and thus further reduces the generation of reactive radicals. Thus, the presence of these co-occurring substances together with their permissible levels on the performance of photocatalytic system has to be determined to ensure minimal disturbances on the efficient operation stability of the TiO_2 based wastewater treatment process. Behnajady et al. [130] examined the effect of bicarbonate and carbonate salts concentration on the photocatalytic degradation of CI. Acid Yellow 23 (AY 23). A large amount of both salts was observed to affect negatively the degradation efficiency. The addition of these salts was reported to block the active sites on ZnO surface thus deactivating the catalyst towards the AY 23 and intermediates molecules. Zhang et al. [158] studied the effect of anions on the photocatalytic degradation of Methyl Orange (MO) which was observed to follow the order of $NO_3^- > SO_4^{2-} > Cl^-$. This was due to the fact that the presence of Cl^- ion can serve as a radical scavenger and reacted with ·OH radicals to form less active $\cdot Cl_2^-$ or $\cdot ClOH^-$ radicals, which restrained the MO degradation dramatically. However, the inhibition effect of SO_4^{2-} ion was attributed to the competition adsorption between anion and reactant for the available ZnO active sites. While NO_3^- was reported without any effect at any concentration up to 0.1 M.

Krishnakumar and Swaminathan [159] considered the influence of inorganic anions on the ZnO photocatalytic degradation of Acid Black 1 (AB 1). They observed that all the inorganic anions were demonstrated to retard the degradation efficiency in the order of $HCO_3^- > CO_3^{2-} > NO-3^- > SO_4^{2-} > Cl^-$. The addition of inorganic anions was reported to affect the photocatalytic activity by competing with dye pollu-

tants to be adsorbed on the catalyst surface and reacting with photo-oxidizing species of ZnO. In the same study [159], the authors further investigated the effect of metal ions on the photocatalytic degradation of AB 1. All the metal ions were found to retard the degradation efficiency in the order of $Mn^{2+} > Cu^{2+} > Ag^{+} > Fe^{2+} > Mg^{2+}$. This retardation effect was explained by the blockage of active sites of ZnO by the deposition of these metal ions on ZnO surface. Addition of dissolved metal ions has been observed to decrease the photocatalytic reaction, whereas other studies have demonstrated a positive effect on the rate of dye pollutants degradation [152,160], hence the effect of metal ions can be varied from dye to dye. Such a positive effect was observed with anionic dye as reported by Khataee and Zarei [152] on the photocatalytic degradation of CI Direct Yellow 12 (DY 12) over immobilized ZnO. At a concentration of 0.1 mM, Fe^{3+} ion was reported to improve the DY 12 degradation as Fe^{3+} ion can trap the photogenerated electrons and the recombination of electron–hole pair thus decreased. They also stated that the introduction of Fe^{3+} ion into the photocatalytic system favoured to activate the H_2O_2 for the formation of ·OH radicals on the surface of ZnO. The effect of transition metal ions has also been investigated by taking different ions such as Fe^{2+}, Ni^{2+}, Ag^{+}, Cu^{2+}, V^{2+}, Co^{2+}, Zn^{2+} and Mn^{2+} on the ZnO photocatalytic degradation of Erythrosin-B, Fast Green FCF and EY [160]. Their results showed that all the dissolved metal ions enhanced the rate of degradation of all three dyes. In the case of Erythrosin-B degradation, the observed order was reported to be $Fe^{2+} > Cu^{2+} > Co^{2+}$, $Mn^{2+} > V^{2+} > Ag^{+} > Ni^{2+} > Zn^{2+}$, and the order was indicated to be $V^{2+} > Co^{2+} > Ag^{+}$, Ni^{2+}, $Cu^{2+} > Zn^{2+} > Mn^{2+}$, Fe^{2+} for the degradation of Fast Green FCF. An order of $V^{2+} > Fe^{2+} > Co^{2+} > Ni^{2+} > Ag^{+} > Mn^{2+} > Zn^{2+} > Cu^{2+}$ was observed for the degradation of EY. The reason given by them was that positively charged metal ions can adsorb on the ZnO surface and consequently, the surface of ZnO became electro-neutral or slightly positively charged. As the three dyes were of anionic nature and thus they can electrostatically attract to the ZnO surface to facilitate the dyes degradation.

The addition of inorganic anions and surfactants on the photocatalytic activity of ZnO has also been studied on the degradation of AO [26]. In their study, the sodium carbonate salt was varied in the range of 2.0×10^{-6}–8.0×10^{-6} M in the AO dye solution of 2.0×10^{-5} M. Their findings revealed that the degradation rate constant, k' value gradually decreased with increasing amounts of carbonate ions. They went further to ascribe this trend to the ·OH radicals scavenging properties of carbonate ions. On the other hand, the influence of sodium chloride on the degradation of AO was carried out in the range 2.0×10^{-3}–1.0×10^{-2} M. The k' value also showed that there was a retrogressive effect on the degradation of AO with increasing in the amount of chloride ions. The decrease in the degradation rate in the presence of chloride ions was due to the photogenerated hole scavenging properties of these ions. The presence of the anionic sodium dodecyl sulphate (SDS) and cationic cetyl trimethylammonium bromide (C_{16}TAB) surfactants was reported to retard the rate of AO degradation. This was due to the preferential adsorption of the amphiphilic surfactant molecules on the ZnO photocatalyst surface. Jiang et al. [89] added the surfactant 1227 and antistatic agent (SN) on the solar photocatalytic degradation of C.I. Basic Blue 41 in an aqueous suspension of TiO_2/ZnO. Under the tested conditions (dye concentration = 20 mg/L, catalyst loading = 10 g/L and solar irradiation time = 1 h), the addition of surfactant 1227 and SN significantly retarded the photocatalytic degradation of CI. Basic Blue 41. The adverse effect was explained by the competition adsorption to the surface of TiO_2/ZnO between CI. Basic Blue 41 and surfactant 1227 or antistatic agent SN due to their similar chemical structures. They also revealed that both additives added to this system can also be photocatalytically degraded by TiO_2/ZnO and thus decreasing the efficiency of dye degradation. On the contrary, a similar negative effect was also observed when the organic solvent such as isopropanol was added into the ZnO photocatalytic degradation system [161]. The presence of 50 mM isopropanol as ·OH radicals scavenger caused a remarkable drop of Fuschine Acid (AV 19) dye degradation efficiency from 75.7 to 19.6%. Daneshvar et al. [132] examined the effect of ethanol in the range 0–9% v/v on the photocatalytic degradation of CI. Acid Orange 7 (AO7) over ZnO. Their results showed that the addition of ethanol restrained the degradation of AO7 because of ·OH radicals competitive reactions between AO7 and ethanol. Thus, the incorporation of a pretreatment process will be required in the photocatalytic textile wastewater treatment so as to reduce the inhibiting effects from the co-occurring substances.

4.7. Effect of oxidizing agents/electron acceptor

In heterogeneous photocatalytic reactions, electron–hole recombination is considered as a major energy wasting step which leads to low quantum yield. Thus, it is crucial to prevent electron–hole recombination to ensure the efficiency of photocatalytic degradation. Molecular oxygen is typically

employed as an effective electron acceptor in most heterogeneous photocatalysed reactions [162,163]. Oxygen can be reduced to the superoxide anions ($O_2^{\cdot-}$), which may also take part in the dye pollutants degradation or be further reacted to form hydrogen peroxide (H_2O_2). Due to the electrophilic property, oxygen plays a vital role in the mechanism of the photocatalytic degradation [27]. Moreover, the enhancement of the photocatalytic efficiency, due to the addition of irreversible oxidizing agents/electron acceptors such as hydrogen peroxide (H_2O_2), persulphate ions ($S_2O_8^{2-}$), bromate ions (BrO_3^-) and oxone ions (HSO_5^-) have been reported by several researchers [55,157,164,165]. The addition of these oxidizing agents enhanced the photocatalytic degradation of dye pollutants by: (i) preventing the electron–hole recombination by accepting the CB electron, (ii) generating more ·OH radicals and other oxidizing species, (iii) accelerating the degradation rate of intermediate compounds and (iv) avoiding low oxygen concentration problems. In most of the cases, the addition of oxidizing agents has resulted in higher dye pollutants degradation rate compared to molecular oxygen. It was demonstrated by Amisha et al. [140] that air (O_2), hydrogen peroxide (H_2O_2) and ammonium persulphate ($(NH_4)_2S_2O_8$) have influence on the degradation of Reactive Black 5 (RB 5) over ZnO under solar and UV light irradiations. The order of enhancement was reported to be $H_2O_2 > (NH_4)_2S_2O_8 > O_2$ in the presence of both solar and UV lights irradiation. The effect of H_2O_2 addition on the photocatalytic degradation of Lissamine Fast Yellow (LFY) over ZnO has also been analysed [166]. They observed that the addition of H_2O_2 enhanced the photocatalytic activity of ZnO from 67 to 84% under visible light irradiation. They added that H_2O_2 has synergetic effect on LFY degradation.

Habib et al. [167] stated that hydrogen peroxide (H_2O_2), ammonium persulphate ($(NH_4)_2S_2O_8$) and potassium bromate ($KBrO_3$) were beneficial for the photocatalytic degradation of Brilliant Golden Yellow. The reactive radical intermediates (·OH, $SO_4^{\cdot-}$ and $BrO_2^{\cdot}$) formed from these oxidizing agents after reaction with the photogenerated electrons can exhibit dual effects: as strong oxidizing agents themselves and as electron scavengers, consequently suppressing the electron–hole recombination at the ZnO surface according to the following equations:

$$H_2O_2 + e^- \rightarrow {}^{\cdot}OH + OH^- \quad (28)$$

$$H_2O_2 + O_2^{\cdot-} \rightarrow {}^{\cdot}OH + OH^- + O_2 \quad (29)$$

$$H_2O_2 + h\nu \rightarrow 2{}^{\cdot}OH \quad (30)$$

$$S_2O_8^- + e^- \rightarrow SO_4^{\cdot-} + SO_4^{2-} \quad (31)$$

$$SO_4^{\cdot-} + H_2O \rightarrow SO_4^{2-} + {}^{\cdot}OH + H^+ \quad (32)$$

$$BrO_3^- + 2H^+ + e^- \rightarrow BrO_2^{\cdot} + H_2O \quad (33)$$

Velmurugan and Swaminathan [55] in their work—ZnO with higher activity in photocatalytic processes, reported on the effect of oxone addition on the photocatalytic degradation of Reactive Red 120 (RR 120) dye. Their results showed that the extent of RR 120 degradation increased from 76.9 to 99.8% with the addition of oxone. They also pointed out that oxone has dual effects on the photocatalytic degradation efficiency of RR 120. The added oxone could accelerate the radical reactions by producing the ·OH and $SO_4^{\cdot-}$ radicals from scavenging the photogenerated electrons as shown by the following reactions:

$$HOOSO_3^- + e^- \rightarrow SO_4^{\cdot-} + OH^- \quad (34)$$

$$HOOSO_3^- + e^- \rightarrow SO_4^{2-} + {}^{\cdot}OH \quad (35)$$

It must be noted that the addition of a requisite amount of the electron acceptors into a photocatalytic system can enhance the dyes degradation efficiency but addition of excess inhibited the dyes degradation. Daneshvar et al. [30] used H_2O_2 to test its effect on photocatalytic degradation of AR 14 under UV-C light irradiation. Their results indicated that there was an optimal concentration of 10 mmol/L H_2O_2, at which the degradation efficiency of AR 14 over the ZnO achieved the maximum. Above the optimum concentration, nevertheless, the excess H_2O_2 was reported to scavenge the ·OH radicals to generate weaker hydroperoxyl radicals ($HO_2^{\cdot}$) and water. Accordingly, the quench ·OH radical effect was given in Eqs. (36) and (37). Due to the decline of the ·OH radicals concentration, the efficiency of AR 14 degradation was retarded at a higher H_2O_2 concentration.

$$ {}^{\cdot}OH + H_2O_2 \rightarrow HO_2^{\cdot} + H_2O \quad (36)$$

$$ {}^{\cdot}OH + HO_2^{\cdot} \rightarrow O_2 + H_2O \quad (37)$$

Furthermore, considering its hydrophilic property, the H_2O_2 also reported to come into contact with the hydroxylated ZnO particles in aqueous solution. Therefore, high concentration of H_2O_2 could suppress the dye degradation efficiency by competing with dye for available ·OH radicals [130,168]. Sobana and Swaminathan et al. [169] investigated the effect of $KBrO_3$ addition from 1 to 4 g/L on the photocatalytic degradation of Acid Red 18 (AR18) using ZnO as catalyst. The addition of $KBrO_3$ from 1 to 3 g/L increased the degradation rate. Further increase of $KBrO_3$ from 3 to 4 g/L decreased the degradation rate. This was due to the adsorption effect of excess Br^- ions on ZnO surface. In the case of sodium persulphate ($Na_2S_2O_8$), a similar observation has been made [50]. This was related to the excess of SO_4^{2-} ions formed during the reaction which can adsorb on the surface of ZnO and deactivate the available ZnO active sites. The optimum concentration of $Na_2S_2O_8$ was found to be 5×10^{-5} M for the efficient dye degradation. Thus, the proper addition of oxidizing agents could accelerate the photocatalytic degradation of dye pollutants. However, in order to maintain the efficiency of the added oxidizing agents, there is the need to consider the proper concentration of oxidizing agents according to the types and the concentrations of the dye pollutants.

5. Multivariate analysis

From the earlier discussions on the effect of the operational parameters on the activities of ZnO-based photocatalysts, it can be found that these parameters would exert their individual influence on the photocatalytic degradation of any dye. Therefore, to study effectively, the photocatalytic degradation of any dye of all the aforementioned parameters must be given consideration. Multivariate analysis is one of the emerging experimental design approaches, which helps to optimize a photocatalytic degradation system since it accounts for interaction effects between the parameters. For the conventional univariate approach, the optimization of photocatalytic degradation system is usually assessed by systematic variation of one parameter while the others are maintained constant. Even though this conventional optimization approach is practically applied, the reported results could be misleading as it partially explores the experimental field and it does not reveal the possible interaction effects between parameters [118].

In this respect, the experimental design approaches such as design of experiment (DOE), response surface analysis and statistical analysis can serve as effective tools for photocatalysis studies. In fact, using the experimental designs allowed to considerable reduction of experiments number and a rapid interpretation of process performance. Compared to the conventional univariate approach for the same number of estimated parameters, experimental design not only can evaluate a large number of parameters but also possibly identify the interaction effects between the tested operating parameters [170]. This permits the process optimization to be more time saving and improves the exploration of experimental field, where it can be analysed using commercial statistical software such as SAS, Minitab and Design Expert.

Annadurai et al. [136] employed Box-Behnken-DOE approach together with analysis of variance, statistical regression and response surface analysis to study the simultaneous effect of dye concentration, ZnO concentration, solution pH and irradiation time on the photocatalytic degradation of CR under solar irradiation. In this approach, 29 experiments were performed based on the combined effects of these four parameters. The results in their report showed that the photocatalytic activity of ZnO was strongly affected by the variations in dye concentration, concentration of ZnO catalyst, solution pH and irradiation time. A response surface model was developed to correlate the degradation rate dependency on the four different parameters according to the statistical regression as follows:

$$Y = b_0 + \sum b_i X_i + \sum \sum_{i \leqslant j} b_{ij} X_i X_j + \sum \sum_{j \leqslant k} \sum b_{ijk} X_i X_j X_k + \varepsilon \quad (38)$$

where Y is the predicted response, i, j and k take values from the number of parameters. b_0 is the constant; b_i represents linear coefficient, b_{ij} and b_{ijk} are quadratic and cubic coefficients where $i = j$ and $i = j = k$, respectively. These refer to interactions of first or second order, respectively, X_i, X_j and X_k are the levels of independent parameters and is the random error. Subsequently, the accuracy and applicability of the model was evaluated by the coefficient of determination R^2 in the analysis of variance (ANOVA). Their results indicated that the experimental values were in good agreement with the predicted values and the R^2 was found to be 0.9982. They further observed that an optimal experimental region was also obtained through the contour and response surface analyses. This was attributed to the experimental design that took both individual and interaction parameters into consideration, which resulted to be more reasonable and beneficial in investigating the photocatalysis

process. Process optimization of the photocatalytic degradation of Reactive Blue 19 (RB 19) using both ZnO and TiO_2 has also analysed using experimental factorial design [171]. The factorial design matrix was built by statistical combinations of the independent parameters of catalyst concentration, solution pH and dye concentration (17 experimental runs for each photocatalyst). Their report also showed that the developed regression equation allowed them to predict and optimized the dye degradation process over ZnO and TiO_2 catalysts. Over the years, other multivariate experimental approaches such as central composite design [172] and D-optimal design [173] have also successfully applied to optimize the photocatalytic degradation system.

6. Synthesis technique and calcination temperature

Various synthesis techniques are available for the preparation of ZnO-based catalysts such as electrochemical, micro-continuous reaction, pulsed laser deposition, thin films and spin coating, thin films by sputtering, dip coating, two-step wet chemical, precipitation, thermal (hydrothermal and solvothermal), combustion, microemulsion, chemical bath deposition, chemical vapour decomposition (CVD), sonochemical, physical vapour deposition (PVD), microwave heating, modified sol–gel and sol–gel [174–192]. Of major interest, sol–gel process is the most commonly used method as it facilitates the synthesis of nanosized crystallized powders at a relatively low temperature, the possibility of stoichiometry controlling process, the preparation of composite materials and the production of homogeneous materials. Depending on the methods of the preparation and the end usage of the ZnO, calcination temperatures have prominent influence on the crystalline size, structure and activity of the prepared catalysts. Thermal treatment of ZnO gels at higher temperature promotes their crystal transformation from amorphous to their crystalline phase such as wurtzite. As dehydration occurs during heat treatment, crystallites grow to dimensions larger than those of the original particles [143]. Muruganandham et al. [193] examined the effect of calcination temperature (400–800°C) on the photocatalytic degradation of MB ZnO nanobundles prepared by thermal decomposition of zinc oxalate. Their XRD results showed that well crystallized, hexagonal wurtize phase ZnO nanobundles were formed at all calcination temperatures. Of all samples tested, the sample calcined at 400°C exhibited the highest photocatalytic activity. This enhancement was related to the formation of well crystallized porous nanobundles and higher adsorption area towards dye pollutant. Increasing the calcination temperature over 400°C caused particle agglomeration resulting in fused nanobundles and thus decreased the photocatalytic activity. Xu et al. [139] considered the effect of calcination temperature on the photocatalytic degradation of C.I. Reactive Blue 4 over sol–gel prepared ZnO nanoparticles supported on sepiolite. In their work, the prepared samples were subjected to various calcination temperatures ranging from 100 to 500°C. Their findings revealed that the catalyst treated at 200°C led to the best enhancement during the degradation of CI. Reactive Blue 4. Fouad et al. [31] studied the effect of calcination temperature on the photocatalytic activity of ZnO thin film synthesized by PVD method for CI. Reactive Black 5 dye degradation. Their results showed that the photocatalytic activity increased in the order of $550 > 650 > 500$° C. High photocatalytic activity for sample calcined at 550°C was explained by the complete growth of ZnO film as indicated by their XRD analysis. On the contrary, the decrease in photocatalytic activity at a higher temperature was ascribed to the reduction of specific surface area as a result of decrease in the percentage of atoms on the catalyst surface due to agglomeration of ZnO grains.

Using flame-spray pyrolysis, Mekasuwandumrong et al. [194] prepared ZnO nanoparticles with annealing post-treatment from 750 to 900°C to be used on the photocatalytic degradation of MB. The results in their report showed that the MB degradation efficiency decreased gradually from 70 to 55% as the annealing temperature increased from 750 to 900°C. As the annealing temperature increased from 750 to 900°C, the resulting ZnO nanoparticles increased their particle sizes from 57.7 to 159.9 nm, whereas BET surface areas decreased from 12 to 5.8 m^2/g. The decrease in photocatalytic degradation efficiency at high annealing temperatures was attributed to large particle size and small surface area, which consequently reduced the adsorption of dye molecules on the catalyst surface. Su et al. [195] investigated the effect of calcination temperature on the photocatalytic degradation of Reactive Brilliance Blue X-BR using ZnO nanoparticles prepared by sol–gel method. The results in their investigation revealed that the prepared ZnO nanoparticles were wurtzite structure attached to hexagonal system. Under the conditions tested, the photocatalytic activity of ZnO nanoparticles increased rapidly and was optimum at 300°C as the calcination temperature increased from 100 to 300°C. Further increase in the calcination temperature from 300 to 600°C, resulted in lower photocatalytic activity of the prepared catalyst.

Behnajady et al. [115] utilized heat attachment method to prepare ZnO nanoparticles immobilized on

glass plate. In their study, the effect of calcination temperature at 400 and 500°C was examined on the photocatalytic degradation of CI. AR88 dye in the presence of UV light irradiation ($\lambda = 254$ nm). Under the conditions tested, the degradation rate constant was observed to decrease from 0.0257 to 0.0208 min^{-1} with increasing calcination temperature from 400 to 500°C. XRD analysis indicated that increasing calcination temperature from 400 to 500°C caused the particle sizes to increase from 42 to 67 nm and therefore reduced the availability of surface area. Yassitepe et al. [196] investigated the efficiency of Reactive Orange (RO 16) and Reactive Red (RR 180) dyes degradation using ZnO plates which sintered at 700 and 1050°C for 1 h. Their results showed that the degradation efficiencies of RO 16 and RR 180 decreased from 88 to 10% and 95 to 8%, respectively, when the sintering temperature was increased from 700 to 1050°C. The larger surface area for sample sintered at 700°C as indicated in their BET analysis was favoured in photocatalytic reactions since the incident UV light can interact with more ZnO surfaces, which led to faster rate of reactions and enhanced dye degradation efficiency. In the presence of ZnO supported on natural zeolites synthesized by hydrothermal method, Delshade et al. [62] tested the influence of calcination temperature (200–500°C) on the photocatalytic degradation of MB. Their results showed that the degradation rate constant increased with calcination temperature and reached a maximum at 400°C. The decrease in the photocatalytic degradation rate for the catalyst treated at higher temperature was due to the aggregation of the ZnO nanoparticles.

7. Analysis and identification of degradation products

Degradation of the wastewaters containing organic dyes is but one central objective of heterogeneous photocatalytic reaction. Total mineralization of the dye is equally crucial for end product. The desired end products for a complete photocatalytic reaction are CO_2 and H_2O. Any nitrogen in the dye (as in the azo compounds) must be similarly converted to N_2, NH_4^+ and NO_3^- ions, chlorine to chloride, sulphur to sulfate, phosphorus to phosphate and so on [63]. Table 4 summarizes the representative studies probing the formation of reaction intermediates during ZnO photocatalytic degradation of various dyes. These include the monitoring of the evolution of CO_2 and the release of inorganic ions from the dye. Determination of the total organic carbon (TOC) and measurement of the COD will reflect the extent of mineralization of the dye. Particularly, total degradation of the dye may still be accompanied by significant residual TOC in the solution, indicating that organic intermediates are generated during the photocatalytic process. Such unintended intermediates can be more toxic than the parent compound which also makes toxicity measurements an obligatory part of the experiments. Two of the popular analysis methods for toxicity measurements are Microtox method using bacteria *Vibrio fischeri* as toxicity indicator and the inhibition of *Escherichia coli* respiration were usually applied in studies dealing with photocatalytic degradation of dyes [29,171,197].

In fact, identification of the reaction intermediates would provide a further insight into the mechanism involved in the photocatalytic degradation process and will help to get a total picture of the process efficacy. Gas chromatography/mass spectroscopy (GC/MS), high performance liquid chromatography (HPLC), high performance liquid chromatography/mass spectroscopy (HPLC/MS), FTIR spectroscopy and UV–vis spectrophotometry are often used to characterize the intermediates of the photocatalytic reaction. The GC/MS is a commonly used method that encompassed a drawback that pre-treatment including a derivatization procedure generally requires several hours to a whole day to be completed [199]. On the contrary, the use of HPLC with various detectors such as UV, fluorescence and electrochemical detection only required a simple and quick pre-treatment method [200]. Among the possible detection methods, MS detection showed significant selectivity to identify accurately and to confirm degradation intermediates. In order to identify abundant intermediates better, electrospray ionization (ESI) source can be used as it causes minimal fragmentation in the dyes. This technique has been used to study the photocatalytic degradation of Basic Blue 11, Ethyl Violet, Methyl Green and Methyl Orange as shown in Table 4. Due to their advantages, the high sensitivity of these techniques combined with the high selectivity allows detection and quantification of intermediates at a very low level of concentration.

8. Into the real world: evaluates with dye wastewaters, solar application and economic consideration

Very few studies of application to real world dye wastewaters with higher degradation efficiency of photocatalytic activity alone can be cited. Additionally, due to the presence of dissolved organic matters in real dye wastewaters, the rates will be substantially lower as compared to that observed in the single-constituent model solution studies. Studies are required

Table 4
Summary of representative studies probing the formation of reaction intermediates during ZnO photocatalytic degradation of various dyes

Dyes	Photocatalyst	Techniques	Comments	References
Reactive Red 120	ZnO	COD measurement, GC–MS	A detailed degradation pathway developed and five main intermediates, namely 2-[(2 hydroxyphenyl)diazenyl]-8-(1,3,5-triazin-2-ylamino)naphthalene-1,3,6-triol, 2,8-diaminonaphthalene-1,3,6-triol, 1,3,5-triazine-2,4-diamine, 2-aminobenzene-1,3-diol and naphthalene-1,2,6,8-tetrol were formed	Velmuruganan and Swaminathan [55]
Remazol Black B and Brilliant Blue R	ZnO	TOC measurement, *E. coli* toxicity test	Presence of residues toxicity together with the permanence of ~20% of original TOC content indicated organic fragments produced at higher photochemical reaction times were toxic	Gouvêa et al. [29]
Reactive Red 180	ZnO	TOC measurement	~90% TOC reduction obtained after 190 min irradiation	Yassitepe et al. [196]
Basic Blue 11	ZnO	TOC measurement, HPLC-PDA-ESI-MS	*N*-de-ethylation and oxidative degradation found to occur in stepwise fashion, sixty-three intermediates were successfully detected, 76.9% TOC reduction was observed	Lu et al. [49]
CI Reactive Blue 4	Nd-ZnO	GC–MS, FTIR spectroscopy	·OH radicals attacked the C-N and C-S bonds on the dye yielding main by-products of 1,3-phenylenediamine, 2,4-dichloride-1,3,5-triazine and 7,10-phenanthrenequinone	Zhou et al. [51]
Ethyl Violet	ZnO	HPLC-PDA-ESI-MS	A detailed degradation pathway discussed including *N*-de-ethylation and oxidative degradation, main products such as mono-, di-, tri-, tetra-, and hexa-ethylated Ethyl Violet species, 4-diethylaminophenol and diethylamino-4′-diethylaminobenzophenone were identified	Chen et al. [24]
Remazol Brilliant Blue R	Ag-ZnO	TOC measurement, *E. coli* toxicity test	~90% TOC reduction obtained after 120 min of photocatalysis and formation of transient toxic species was observed.	Gouvêa et al. [197]
Methyl Orange	ZnO	HPLC-MS, UV–vis spectrophotometry	Aromatic intermediates such as $C_{13}H_{13}N_3O_3S$, $C_{12}H_{11}N_3O_3S$, $C_{13}H_{13}N_3O$, $C_{14}H_{15}N_3O_4S$, $C_{13}H_{13}N_3O_4S$, $C_{14}H_{15}N_3O$ and $C_7H_7NO_2$ were detected	Comparelli et al. [54]
Methyl Red	ZnO/glass	HPLC-UV-MS	Two different mechanisms found in the degradation pathway identifying the occurrence of degradation intermediates such as $C_{14}H_{13}N_3O_2$, $C_{13}H_{11}N_3O_2$, $C_{14}H_{13}N_3O_3$, $C_{14}H_{13}N_3O_4$, $C_{15}H_{15}N_3O_3$ and $C_{15}H_{15}N_3O_5$	Comparelli et al. [53]
Methyl Green	ZnO	HPLC-photodiode array-ESI-MS	A multiplicity of pathways including *N*-de-ethylation and oxidative degradation, 32 intermediates were identified	Mai et al. [50]
Acid Red 27	ZnO/glass plates	UV–vis spectrophotometry, COD measurement	UV–vis spectra during reaction indicated formation of inorganic ions such as SO_4^{2-}, NH_4^+, $NO_3^-$and NO_2^-	Behnajady et al. [154]
Procion Blue HERD	ZnO	COD measurement, GC–MS	Dye degradation accompanied by COD reduction and formation of smaller organic intermediates with retention time 39.25 and 41.97 min	Bansal and Sud [138]
Aridine Orange	ZnO	COD measurement, UV–vis spectrophotometry, CO_2 analyses by added limewater	CO_2 evolution found concomitantly with the photocatalytic degradation of dye	Pare et al. [26]
Reactive Blue 19	ZnO	TOC measurement, Microtox toxicity test	~ 60% TOC reduction obtained with almost complete removal of acute toxicity after 1 h irradiation	Lizama et al. [171]
Methyl Orange	Ag–ZnO	HPLC–ESI-MS, UV–vis spectrophotometry	Progressively demethylated products found, four intermediates identified with molecular weight MS 276, 290, 306 and 320	Chen et al. [52]

(*Continued*)

Table 4 (*continued*)

Dyes	Photocatalyst	Techniques	Comments	References
Safranin T	ZnO/MoO_3	COD and TOC measurements, FTIR spectroscopy	Degradation efficiency and COD reached above 98% and 95%, respectively. Dye was totally mineralized to inorganic species such as HCO_3^-, Cl^- and NO_3^-	Huang et al. [90]
Orange II	ZnO	TOC measurement	Complete degradation and mineralization achieved at 60 and 300 min, respectively	Nishio et al. [32]
Rhodamine B and Methyl Orange	ZnO/ polymer	TOC measurement	Degradation of the xanthene ring structure more effective than that of the azo group	Qiu et al. [46]
Methylene Blue	Sn-ZnO	COD and TOC measurements	Complete COD and TOC removals observed after 10 h	Sun et al. [94]
Biebrich Scarlet	ZnO	COD measurement	COD reduction lay between 90 and 92% after 20 min indicated the formation smaller uncoloured products	Kansal et al. [45]
Eosin Y	ZnO	TOC measurement, Br ion analyses by conductivity measurement	Br ion released along with CO_2 formation concomitantly with the dye degradation	Poulios et al. [198]

for testing photocatalytic degradation for a variety of simulated wastewaters containing mixture of dye components and the concentration of the dissolved organic matters as well as other co-occurring substances including salt (as described above) that affect the rates. Furthermore, the characteristics of real world dye wastewater such as TOC, COD, BOD, TDS and pH samples should be identified and elucidated.

Bansal and Sud [138] studied the effectiveness of ZnO photocatalytic treatment on Procion yellow HERD reactive dye in both synthetic effluent and real effluent from textile industry. Under the conditions tested, degradation of textile effluent took place and a significant decrease in the COD value of effluent with respect to its initial COD value was observed, indicating the removal of recalcitrant organic compounds from textile mill effluent. However, in comparing this result with that of the solution of pure synthetic dye, they reported that the degradation efficiency of the real textile effluent was relatively lower than that of the pure synthetic dye. In a photocatalysis study on real textile effluent sample containing the Procion Yellow H-EXL reactive dye, Barakat [201] also found that the degradation of real textile effluent went on at a slower rate compared to the pure synthetic dye. This retardation was attributed to the presence of some impurities such as dissolved organic substances and chloride ions as indicated in the real textile effluent sample which interfered with the Procion Yellow H-EXL during the degradation processes. Kansal et al. [202] examined the efficiencies of ZnO on the photocatalytic degradation of bleach plant effluents. Noticeable decrease in the COD and BOD values of effluents were reported under both UV and solar irradiation. Roselin and Selvin [203] studied the photocatalytic degradation of actual cotton dyeing effluent using ZnO as a catalyst. The results in their study revealed that the trade effluent having an initial COD value of 685 mg/L was reduced to 18.3 mg/L on exposure to solar irradiation for 2.5 h. Silk industrial effluents containing amaranth acid dye as a major constituent with other dyes and dyeing auxiliaries have also been considered for the photocatalytic degradation using ZnO nanoparticles coated onto the surface of calcium alumino silicate beads [204]. The increase in degradation efficiency and reduction in rate of COD were observed, demonstrating the disappearance of colour of dye molecules and destruction of organic molecules in the effluents.

Switching focus to solar application efforts, several key technical constraints ranging from catalyst development to reactor configuration have to be addressed. These include (i) catalyst improvement for a high photocatalytic efficiency that can utilize wide solar spectra and (ii) effective configuration of photocatalytic reactor system for higher utilization of solar application. For the catalyst development, great efforts such as ions and metal oxides doping (Sections 3.2–3.4) have been spent to prevent the recombination of charge carrier in the catalyst and to improve the photocatalytic efficiency of ZnO into visible region, especially under solar light irradiation. While such modifications have demonstrated significant improvement in the ability of ZnO system to remediate wastewater in laboratory scale, it is apparent that the need to develop pilot scale treatment systems and to apply this technique in cost effective dyehouse effluent purification processes. Modeling and reactor design are critical for successful industrial application. In this regard, different kinds of solar reactors have been proposed such as parabolic trough reactor (PTR), compound parabolic collecting reactor (CPCR), double skin sheet reactor (DSSR) and thin film fixed bed reactor for the photocatalytic studies [205–207]. Design efficiency for a reactor

configuration is mainly dependent upon its ability to install as much catalyst per unit volume as possible a factor necessary for scale-up [28]. Thus, more work is needed in the fundamentals of reactor design and optimization of heterogeneous photocatalytic reactors.

Besides these, in heterogeneous photocatalytic degradation of organic dyes, the photon generation driven by UV and/or solar light for catalyst activation is the significant part of the total cost for the operation of the system. The evaluation of the treatment cost is, at this time, one of the aspects that need more attention. Accordingly, the Photochemistry commission of the International Union of Pure and Applied Chemistry (IUPAC) has proposed a figure-of-merit that can provide a direct relation to the electric- or solar-energy efficiency of an AOP. The figure-of-merit is the "electrical energy per order" (E_{EO}), defined as the number of kilowatt hour (kWh) of electrical energy required to degrade the concentration of a pollutant by one order of magnitude (90%) in 1,000 L of contaminated water [208]. Several researchers have evaluated the energy efficiency of the photocatalytic water purification system for degradation of various organic contaminants in water [132,171,208,209]. Lizama et al. [171] evaluated the E_{EO} for the photocatalytic degradation of the Reactive Blue 19. Their results showed that in the case of the UV/TiO_2 process, the E_{EO} value was reported to be 22.4 kWh/m^3 compared to 7.6 kWh/m^3 in the UV/ZnO system. Daneshvar et al. [132] revealed that the CI. Acid Orange 7 could be treated easily and effectively using an UV/ZnO/H_2O_2 system with an E_{EO} value of 172 kWh/m^3. They added that the use of H_2O_2 with an optimum concentration of 10 mM in the UV/ZnO can be extremely helpful in reducing the energetic cost of real wastewater treatment. The E_{EO} calculation is decisive however, the costs associated with chemicals and capital outlays should also be considered to gain an overall comparative picture of the process economics.

9. Conclusion and outlook

ZnO has long been used to remediate organic pollutants present in wastewater. Consequently, significant effort has been directed during the last several years on the photocatalytic technologies of various classes of organic dyes degradation towards this semiconductor material. In this review, we have revealed various ways of ZnO-based catalysts modification successfully utilized for the photocatalytic degradation of organic dyes, especially aiming at high efficiency and activity in visible region, even for solar irradiation. Modifications have been achieved using ZnO nanostructures, semiconductor coupling, metal and non-metal doping. The reported findings also suggested that numerous operational parameters such as type of organic substrate and its concentration, amount of catalyst, light intensity and wavelength, solution pH, co-occurring substances in water and oxidizing agents/electron acceptors can considerably affect the degradation and mineralization efficiencies of organic dyes. Optimization of the operational parameters is of paramount importance from the design and the operational points of view when selecting a sustainable and competent technique for the wastewater treatment processes. It has also been discovered that many synthesis techniques are used in the preparation of ZnO-based catalysts and an optimum temperature at which the catalyst must be calcined is crucial. By the detailed elucidation on the analysis and identification of degradation products of the organic dyes, this review can also provide theoretic evidences for seeking new and high efficiency of photocatalytic reactions for organic dyes. The application of ZnO-based catalyst photocatalytic technique under multi-components of organic dyes calls for further investigation as the organic dyes in the real world wastewater are in the form of mixture. Additionally, most of the photocatalytic studies concentrated only on the degradation rate and efficiency of target organic dyes disregarding the toxicity issues of the degradation intermediates. This aspect should not be overlooked while reporting any future work. A demonstrated ability to use ZnO-based catalyst at a solar pilot scale for effluent purification processes would certainly benefit the commercial sector both in terms of environment and economy. Although this review is non-exhaustive in the scope of photocatalytic degradation of organic dyes, it does however address the fundamental principles and application in this area.

Acknowledgement

This study is supported by a Research Universiti (RU) Grant (No. 854001) from Universiti Sains Malaysia. The authors gratefully acknowledge the financial support from the Malaysia Government through the MyPhD scheme.

References

[1] C.A. Martínez-Huitle, E. Brillas, Decontamination of wastewaters containing synthetic organic dyes by electrochemical methods: A general review, Appl. Catal. B: Environ. 87 (2009) 105–145.

[2] I.H. Cho, K.D. Zoh, Photocatalytic degradation of azo dye (Reactive Red 120) in TiO_2/UV system: Optimization and modeling using a response surface methodology (RSM) based on the central composite design, Dyes Pigments 75 (2007) 533–543.

[3] B.K. Körbahti, A. Tanyolac, Electrochemical treatment of simulated textile wastewater with industrial components and Levafix Blue CA reactive dye: Optimization through response surface methodology, J. Hazard. Mater. 151 (2008) 422–431.
[4] A.R. Khataee, M. Zarei, L. Moradkhannejhad, Application of response surface methodology for optimization of azo dye removal by oxalate catalyzed photoelectro-Fenton process using carbon nanotube-PTFE cathode, Desalination 258 (2010) 112–119.
[5] K.Y. Foo, B.H. Hameed, Decontamination of textile wastewater via TiO_2/activated carbon composite materials, Adv. Colloid. Interface Sci. 159 (2010) 130–143.
[6] B.H. Hameed, U.G. Akpan, K.P. Wee, Photocatalytic degradation of Acid Red 1 dye using ZnO catalyst in the presence and absence of silver, Desalin. Water Treat. 27 (2011) 204–209.
[7] M.N. Chong, B. Jin, C.W.K. Chow, C. Saint, Recent developments in photocatalytic water treatment technology: A review, Water Res. 44 (2010) 2997–3027.
[8] A. Sotto, M.J. López-Muñoz, J.M. Arsuaga, J. Aguado, A. Revilla, Membrane treatment applied to aqueous solutions containing atrazine photocatalytic oxidation products, Desalin. Water Treat. 21 (2010) 175–180.
[9] D. Chatterjee, S. Dasgupta, Visible light induced photocatalytic degradation of organic pollutants, J. Photochem. Photobio. C: Photochem. Rev. 6 (2005) 186–205.
[10] R.M. Christie, Environmental Aspects of Textile Dyeing, CRC Press, Cambridge, 2007.
[11] K. Hunger, Industrial Dyes: Chemistry, Properties, Applications, Wiley-VCH, Cambridge, 2003.
[12] E.N. Abrahart, Dyes and Their Intermediates, Edward Arnold, New York, NY, 1977.
[13] V.K. Gupta, Suhas Application of low-cost adsorbents for dye removal—a review, J. Environ. Manage. 90 (2009) 2313–2342.
[14] C.A. Harper, Guide to Ceramic Materials. Handbook of Ceramics, Glasses, and Diamonds, McGraw-Hill, New York, NY, 2001.
[15] F. Porter, Zinc Dust and Compounds. Zinc Handbook Properties, Processing, and Use in Design, Marcel Dekker, New York, NY, 1991.
[16] Z.L. Wang, Zinc oxide nanostructures: Growth, properties and applications, J. Phys.: Condens. Matter 16 (2004) R829–R858.
[17] S. Baruah, J. Dutta, Hydrothermal growth of ZnO nanostructures, Sci. Technol. Adv. Mater. (2009) 101–118.
[18] Ü. Özgür, Y.I. Alivov, C. Liu, A. Teke, M.A. Reshchikov, S. Doğan, V. Avrutin, S.J. Cho, H. Morkoçd, A comprehensive review of ZnO materials and devices, J. Appl. Phys. 98 (2005) 1–103.
[19] A. Janotti, C.G. Van de Walle, Fundamentals of zinc oxide as a semiconductor, Rep. Prog. Phys. 72 (2009) 1–29.
[20] S. Rehman, R. Ullah, A.M. Butt, N.D. Gohar, Strategies of making TiO_2 and ZnO visible light active, J. Hazard. Mater. 170 (2009) 560–569.
[21] M.D. Hernández-Alonso, F. Fresno, S. Suárez, J.M. Coronado, Development of alternative photocatalysts to TiO_2: Challenges and opportunities, Energy Environ. Sci. 2 (2009) 1231–1257.
[22] S. Malato, P. Fernández-Ibánez, M.I. Maldonado, J. Blanco, W. Gernjak, Decontamination and disinfection of water by solar photocatalysis: Recent overview and trends, Catal. Today 147 (2009) 1–59.
[23] S. Sakthivel, B. Neppolian, M.V. Shankar, B. Arabindoo, M. Palanichamy, V. Murugesan, Solar photocatalytic degradation of azo dye: Comparison of photocatalytic efficiency of ZnO and TiO2, Solar Energy Mater. Solar Cells 77 (2003) 65–82.
[24] C.C. Chen, Degradation pathways of ethyl violet by photocatalytic reaction with ZnO dispersions, J. Mol. Catal. A: Chem. 264 (2007) 82–92.
[25] S.K. Kansal, M. Singh, D. Sud, Studies on photodegradation of two commercial dyes in aqueous phase using different photocatalysts, J. Hazard. Mater. 141 (2007) 581–590.
[26] B. Pare, S.B. Jonnalagadda, H. Tomar, P. Singh, V.W. Bhagwat, ZnO assisted photocatalytic degradation of acridine orange in aqueous solution using visible irradiation, Desalination 232 (2008) 80–90.
[27] O. Carp, C.L. Huisman, A. Reller, Photoinduced reactivity of titanium dioxide, Prog. Solid State Chem. 32 (2004) 33–177.
[28] U.I. Gaya, A.H. Abdullah, Heterogeneous photocatalytic degradation of organic contaminants over titanium dioxide: A review of fundamentals, progress and problems, J. Photochem. Photobio. C: Photochem. Rev. 9 (2008) 1–12.
[29] C.A.K. Gouvéa, F. Wypych, S.G. Moraes, N. Durán, N. Nagata, P. Peralta-Zamora, Semiconductor-assisted photocatalytic degradation of reactive dyes in aqueous solution, Chemosphere 40 (2000) 433–440.
[30] N. Daneshvar, D. Salari, A.R. Khataee, Photocatalytic degradation of azo dye acid red 14 in water on ZnO as an alternative catalyst to TiO_2, J. Photochem. Photobio. A: Chem. 162 (2004) 317–322.
[31] O.A. Fouad, A.A. Ismail, Z.I. Zaki, R.M. Mohamed, Zinc oxide thin films prepared by thermal evaporation deposition and its photocatalytic activity, Appl. Catal. B: Environ. 62 (2006) 144–149.
[32] J. Nishio, M. Tokumura, H.T. Znad, Y. Kawase, Photocatalytic decolorization of azo-dye with zinc oxide powder in an external UV light irradiation slurry photoreactor, J. Hazard. Mater. 138 (2006) 106–115.
[33] S.K. Kansal, N. Kaur, S. Singh, Photocatalytic degradation of two commercial reactive dyes in aqueous phase using nanophotocatalysts, Nanoscale Res. Lett. 4 (2009) 709–716.
[34] Q.Y. Li, C.L. Wang, M.L. Ju, W.L. Chen, E.B. Wang, Polyoxometalate-assisted electrochemical deposition of hollow ZnO nanospheres and their photocatalytic properties, Micropor. Mesopor. Mater. 138 (2011) 132–139.
[35] N. Modirshahla, A. Hassani, M.A. Behnajady, R. Rahbarfam, Effect of operational parameters on decolorization of Acid Yellow 23 from wastewater by UV irradiation using ZnO and ZnO/SnO_2 photocatalysts, Desalination 271 (2011) 187–192.
[36] M. Samah, S. Merabet, M. Bouguerra, M. Bouhelassa, S. Ouhenia, A. Bouzaza, Photo-oxidation process of indole in aqueous solution with ZnO catalyst: study and optimization, Kinet. Catal. 52 (2011) 34–39.
[37] A. Mills, S. Le Hunte, An overview of semiconductor photocatalysis, J. Photochem. Photobio. A: Chem. 108 (1997) 1–35.
[38] M.R. Hoffmann, S.T. Martin, W.Y. Choi, D.W. Bahnemann, Environmental applications of semiconductor photocatalysis, Chem. Rev. 95 (1995) 69–96.
[39] S.M. Chang, P.H. Lo, C.T. Chang, Photocatalytic behavior of TOPO-capped TiO_2 nanocrystals for degradation of endocrine disrupting chemicals, Appl. Catal. B: Environ. 91 (2009) 619–627.
[40] Q. Xiao, Z.C. Si, J. Zhang, C. Xiao, X.K. Tan, Photoindued hydroxyl radical and photocatalytic activity of samarium-doped TiO_2 nanocrystalline, J. Hazard. Mater. 150 (2008) 62–67.
[41] Y.X. Li, J.X. Wang, S.Q. Peng, G.X. Lu, S.B. Li, Photocatalytic hydrogen generation in the presence of glucose over ZnS-coated $ZnIn2S_4$ under visible light irradiation, Inter. J. Hydrogen Energy 35 (2010) 7116–7126.
[42] Q.J. Xiang, J.G. Yu, P.K. Wong, Quantitative characterization of hydroxyl radicals produced by various photocatalysts, J. Colloid Interf. Sci. 357 (2011) 163–167.
[43] G.M. Liu, J.C. Zhao, H. Hidaka, ESR spin-trapping detection of radical intermediates in the TiO_2-assisted photo-oxidation of sulforhodamine B under visible irradiation, J. Photochem. Photobio. A: Chem. 133 (2000) 83–88.
[44] H.B. Fu, L.W. Zhang, S.C. Zhang, Y.F. Zhu, J.C. Zhao, Electron spin resonance spin-trapping detection of radical intermediates in N-doped TiO_2-assisted photodegradation of 4-chlorophenol, J. Phys. Chem. B 110 (2006) 3061–3065.

[45] X.J. Ding, T.C. An, G.Y. Li, J.X. Chen, G.Y. Sheng, J.M. Fu, J.C. Zhao, Photocatalytic degradation of dimethyl phthalate ester using novel hydrophobic TiO_2 pillared montmorillonite photocatalyst, Res. Chem. Intermediates 34 (2008) 67–83.
[46] R.L. Qiu, D.D. Zhang, Y.Q. Mo, L. Song, E. Brewer, X.F. Huang, Y. Xiong, Photocatalytic activity of polymer-modified ZnO under visible light irradiation, J. Hazard. Mater. 156 (2008) 80–85.
[47] Y.B. Xie, C.W. Yuan, X.Z. Li, Photosensitized and photocatalyzed degradation of azo dye using $Ln^{n+}-TiO_2$ sol in aqueous solution under visible light irradiation, Mater. Sci. Eng. B 117 (2005) 325–333.
[48] J.F. Guo, J.X. Li, A.Y. Yin, K.N. Fan, W.L. Dai, Photodegradation of Rhodamine B on sulfur doped ZnO/TiO_2 nanocomposite photocatalyst under visible-light irradiation, Chin. J. Chem. 28 (2010) 2144–2150.
[49] C.S. Lu, Y.T. Wu, F. Mai, W.S. Chung, C.W. Wu, W.Y. Lin, C. C. Chen, Degradation efficiencies and mechanisms of the ZnO-mediated photocatalytic degradation of Basic Blue 11 under visible light irradiation, J. Mol. Catal. A: Chem. 310 (2009) 159–165.
[50] F.D. Mai, C.C. Chen, J.L. Chen, S.C. Liu, Photodegradation of methyl green using visible irradiation in ZnO suspensions determination of the reaction pathway and identification of intermediates by a high-performance liquid chromatography–photodiode array-electrospray ionization-mass spectrometry method, J. Chromatogr. A 1189 (2008) 355–365.
[51] Y. Zhou, S.X. Lu, W.G Xu, Photocatalytic activity of Nd-doped ZnO for the degradation of CI Reactive Blue 4 in aqueous suspension, Environ. Prog. Sustainable Energy 28 (2009) 226–233.
[52] T.W. Chen, Y.H. Zheng, J.M. Lin, G.N. Chen, Study on the photocatalytic degradation of methyl orange in water using Ag/ZnO as catalyst by liquid chromatography electrospray ionization ion-trap mass spectrometry, J. Am. Soc. Mass Spectrom. 19 (2008) 997–1003.
[53] R. Comparelli, P.D. Cozzoli, M.L. Curri, A. Agostiano, G. Mascolo, G. Lovecchio, Photocatalytic degradation of methyl-red by immobilised nanoparticles of TiO_2 and ZnO, Water Sci. Techol. 49 (2004) 183–188.
[54] R. Comparelli, E. Fanizza, M.L. Curri, P.D. Cozzoli, G. Mascolo, A. Agostiano, UV-induced photocatalytic degradation of azo dyes by organic-capped ZnO nanocrystals immobilized onto substrates, Appl. Catal. B: Environ. 60 (2005) 1–11.
[55] R. Velmurugan, M. Swaminathan, An efficient nanostructured ZnO for dye sensitized degradation of Reactive Red 120 dye under solar light, Solar Energy Mater. Solar Cells 95 (2011) 942–950.
[56] K.V. Kumar, K. Porkodi, A. Selvaganapathi, Constrain in solving Langmuir–Hinshelwood kinetic expression for the photocatalytic degradation of Auramine O aqueous solutions by ZnO catalyst, Dyes Pigm. 75 (2007) 246–249.
[57] H.W. Yan, J.B. Hou, Z.P. Fu, B.F. Yang, P.H. Yang, K.P. Liu, M.W. Wen, Y.J. Chen, S.Q. Fu, F.Q. Li, Growth and photocatalytic properties of one-dimensional ZnO nanostructures prepared by thermal evaporation, Mater. Res. Bull. 44 (2009) 1954–1958.
[58] J. Bandara, K. Tennakone, P.P.B. Jayatilaka, Composite tin and zinc oxide nanocrystalline particles for enhanced charge separation in sensitized degradation of dyes, Chemosphere 49 (2002) 439–445.
[59] S. Chakrabarti, B.K. Dutta, Photocatalytic degradation of model textile dyes in wastewater using ZnO as semiconductor catalyst, J. Hazard. Mater. 112 (2004) 269–278.
[60] N. Sobana, M. Swaminathan, Combination effect of ZnO and activated carbon for solar assisted photocatalytic degradation of Direct Blue 53, Solar Energy Mater. Solar Cells 91 (2007) 727–734.
[61] J.Z. Kong, A.D. Li, X.Y. Li, H.F. Zhai, W.Q. Zhang, Y.P. Gong, H. Li, D. Wu, Photo-degradation of methylene blue using Ta-doped ZnO nanoparticles, J. Solid State Chem. 183 (2010) 1359–1364.
[62] E. Sanatgar-Delshade, A. Habibi-Yangjeh, M. Khodadadi-Moghaddam, Hydrothermal low-temperature preparation and characterization of ZnO nanoparticles supported on natural zeolite as a highly efficient photocatalyst, Monatsh. Chem. 142 (2011) 119–129.
[63] I.K. Konstantinou, T.A. Albanis, TiO_2-assisted photocatalytic degradation of azo dyes in aqueous solution: Kinetic and mechanistic investigations. A review, Appl. Catal. B: Environ. 49 (2004) 1–14.
[64] F.F. Brites, V.S. Santana, N.R.C. Fernandes-Machado, Effect of support on the photocatalytic degradation of textile effluents using Nb_2O_5 and ZnO: Photocatalytic degradation of textile dye, Top. Catal. 54 (2011) 264–269.
[65] Q.F. Zhang, G.Z. Cao, Nanostructured photoelectrodes for dye-sensitized solar cells, Nano Today 6 (2011) 91–109.
[66] X.S. Fang, T.Y. Zhai, U.K. Gautam, L. Li, L.M. Wu, Y. Bando, D. Golberg, ZnS nanostructures: From synthesis to applications, Prog. Mater. Sci. 56 (2011) 175–287.
[67] W.S. Chiu, P.S. Khiew, M. Cloke, D. Isa, T.K. Tan, S. Radiman, R. Abd-Shukor, M.A. Abd. Hamid, N.M. Huang, H.N. Lim, C.H. Chia, Photocatalytic study of two-dimensional ZnO nanopellets in the decomposition of methylene blue, Chem. Eng. J. 158 (2010) 345–352.
[68] L. Zhang, H.Q. Yang, J.H. Ma, L. Li, X.W. Wang, L.H. Zhang, S. Tian, X.Y. Wang, Controllable synthesis and shape-dependent photocatalytic activity of ZnO nanorods with a cone and different aspect ratios and of short-and-fat ZnO microrods by varying the reaction temperature and time, Appl. Phys. Astronomy 100 (2010) 106–1067.
[69] A. Umar, Growth of comb-like ZnO nanostructures for dye-sensitized solar cells applications, Nanoscale Res. Lett. 4 (2009) 1004–1008.
[70] M.S. Mohajerani, A. Lak, A. Simchi, Effect of morphology on the solar photocatalytic behavior of ZnO nanostructures, J. Alloys Compounds 485 (2009) 616–620.
[71] Y.C. Lu, L.L. Wang, D.J. Wang, T.F. Xie, L.P. Chen, Y.H. Lin, A comparative study on plate-like and flower-like ZnO nanocrystals surface photovoltage property and photocatalytic activity, Mater. Chem. Phys. 129 (2011) 281–287.
[72] Q.Y. Zhu, J. Chen, Q. Zhu, Y.M. Cui, L. Liu, B. Li, X.F. Zhou, Monodispersed hollow microsphere of ZnO mesoporous nanopieces: Preparation, growth mechanism and photocatalytic performance, Mater. Res. Bull. 45 (2010) 2024–2030.
[73] S.S. Warule, N.S. Chaudhari, B.B. Kale, M.A. More, Novel sonochemical assisted hydrothermal approach towards the controllable synthesis of ZnO nanorods, nanocups and nanoneedles and their photocatalytic study, Cryst. Eng. Comm. 11 (2009) 2776–2783.
[74] A. Umar, M.S. Chauhan, S. Chauhan, R. Kumar, G. Kumar, S. A. Al-Sayari, S.W. Hwang, A. Al-Hajry, Large-scale synthesis of ZnO balls made of fluffy thin nanosheets by simple solution process: Structural, optical and photocatalytic properties, J. Colloid Interf. Sci. 363 (2011) 521–528.
[75] S. Baruah, C. Thanachayanont, J. Dutta, Growth of ZnO nanowires on nonwoven polyethylene fibers, Sci. Technol. Adv. Mater. 9 (2008) 1–8.
[76] C.H. Ye, Y. Bando, G.Z. Shen, D. Golberg, Thickness-dependent photocatalytic performance of ZnO nanoplatelets, J. Phys. Chem. B 110 (2006) 15146–15151.
[77] J. Xie, Y.T. Li, W. Zhao, L. Bian, Y. Wei, Simple fabrication and photocatalytic activity of ZnO particles with different morphologies, Powder Technol. 207 (2011) 140–144.
[78] S.S. Ma, R. Li, C.P. Lv, W. Xu, X.L. Gou, Facile synthesis of ZnO nanorod arrays and hierarchical nanostructures for photocatalysis and gas sensor applications, J. Hazard. Mater. 192 (2011) 730–740.

[79] S.K. Kansal, A.H. Ali, S. Kapoor, D.W. Bahnemann, Synthesis of flower like zinc oxide nanostructure and its application as a photocatalyst, Sep. Purif. Technol. 80 (2011) 125–130.
[80] Y.C. Chen, S.L. Lo, Effects of operational conditions of microwave-assisted synthesis on morphology and photocatalytic capability of zinc oxide, Chem. Eng. J. 170 (2011) 411–418.
[81] J.H. Yan, L. Zhang, H.H. Yang, Y.G. Tang, Z.G. Lu, S.L. Guo, Y.L. Dai, Y. Han, M.H. Yao, $CuCr_2O_4/TiO_2$ heterojunction for photocatalytic H_2 evolution under simulated sunlight irradiation, Sol. Energy 83 (2009) 1534–1539.
[82] P. Sathishkumar, R. Sweena, J.J. Wu, S. Anandan, Synthesis of CuO–ZnO nanophotocatalyst for visible light assisted degradation of a textile dye in aqueous solution, Chem. Eng. J. 171 (2011) 136–140.
[83] S.Q. Wei, Z.C. Shao, X.D. Lu, Y. Liu, L.L. Cao, Y. He, Photocatalytic degradation of methyl orange over ITO/CdS/ZnO interface composite films, J. Environ. Sci. 21 (2009) 991–996.
[84] R. Saravanan, H. Shankar, T. Prakash, V. Narayanan, A. Stephen, ZnO/CdO composite nanorods for photocatalytic degradation of methylene blue under visible light, Mater. Chem. Phys. 125 (2011) 277–280.
[85] W. Yan, H.Q. Fan, C. Yang, Ultra-fast synthesis and enhanced photocatalytic properties of alpha-Fe_2O_3/ZnO core-shell structure, Mater. Lett. 65 (2011) 1595–1597.
[86] C. Wang, X.M. Wang, B.Q. Xu, J.C. Zhao, B.X. Mai, P. Peng, G.Y. Sheng, J.M. Fu, Enhanced photocatalytic performance of nanosized coupled ZnO/SnO_2 photocatalysts for methyl orange degradation, J. Photochem. Photobio. A: Chem. 168 (2004) 47–52.
[87] H.C. Ma, J.H. Han, Y.H. Fu, Y. Song, C.L. Yu, X.L. Dong, Synthesis of visible light responsive ZnO–ZnS/C photocatalyst by simple carbothermal reduction, Appl. Catal. B: Environ. 102 (2011) 417–423.
[88] C.R. Li, R. Chen, X.Q. Zhang, S.X. Shu, J. Xiong, Y.Y. Zheng, W.J. Dong, Electrospinning of CeO_2–ZnO composite nanofibers and their photocatalytic property, Mater. Lett. 65 (2011) 1327–1330.
[89] Y.H. Jiang, Y.M. Sun, H. Liu, F.H. Zhu, H.B Yin, Solar photocatalytic decolorization of CI Basic Blue 41 in an aqueous suspension of TiO_2–ZnO, Dyes Pigm. 78 (2008) 77–83.
[90] J.G. Huang, X.H. Wang, S. Li, Y. Wang, ZnO/MoO_3 mixed oxide nanotube: A highly efficient and stable catalyst for degradation of dye by air under room conditions, Appl. Surf. Sci. 257 (2010) 116–121.
[91] C.L. Yu, K. Yang, Q. Shu, J.C. Yu, F.F. Cao, X. Li, Preparation of WO_3/ZnO composite photocatalyst and its photocatalytic performance, Chin. J. Catal. 32 (2011) 555–565.
[92] L.S. Wang, M.W. Xiao, X.J. Huang, Y.D. Wu, Synthesis, characterization, and photocatalytic activities of titanate nanotubes surface-decorated by zinc oxide nanoparticles, J. Hazard. Mater. 161 (2009) 49–54.
[93] J.H. Sun, S.Y. Dong, J.L. Feng, X.J. Yin, X.C. Zhao, Enhanced sunlight photocatalytic performance of Sn-doped ZnO for Methylene Blue degradation, J. Mol. Catal. A: Chem. 335 (2011) 145–150.
[94] D. Jackson and S.J. Hargreaves, Oxide Materials in Photocatalytic Processes. Metal Oxide Catalysis, Wiley-VCH, Weinheim, 2009.
[95] S.Y. Gao, X.X. Jia, S.X. Yang, Z.D. Li, K. Jiang, Hierarchical Ag/ZnO micro/nanostructure: green synthesis and enhanced photocatalytic performance, J. Solid State Chem. 184 (2011) 764–769.
[96] T.K. Jia, W.M. Wang, F. Long, Z.Y. Fu, H. Wang, Q.J. Zhang, Fabrication, characterization and photocatalytic activity of La-doped ZnO nanowires, J. Alloys Compounds 484 (2009) 410–415.
[97] J.Z. Kong, A.D. Li, H.F. Zhai, Y.P. Gong, H. Li, D. Wu, Preparation, characterization of the Ta-doped ZnO nanoparticles and their photocatalytic activity under visible-light illumination, J. Solid State Chem. 182 (2009) 2061–2067.
[98] C.L. Wu, L. Shen, Y.C. Zhang, Q.L. Huang, Solvothermal synthesis of Cr-doped ZnO nanowires with visible light-driven photocatalytic activity, Mater. Lett. 65 (2011) 1794–1796.
[99] C. Xu, L.X. Cao, G. Su, W. Liu, X.F. Qu, Y.Q. Yu, Preparation, characterization and photocatalytic activity of Co-doped ZnO powders, J. Alloys Compounds 497 (2010) 373–376.
[100] C.L. Wu, Q.L. Huang, Synthesis of Na-doped ZnO nanowires and their photocatalytic properties, J. Luminescence 130 (2010) 2136–2141.
[101] P. Li, Z. Wei, T. Wu, Q. Peng, Y.D. Li, Au–ZnO hybrid nanopyramids and their photocatalytic properties, J. Am. Chem. Soc. 133 (2011) 5660–5663.
[102] R. Slama, F. Ghribi, A. Houas, C. Barthou, L. El Mir, Visible photocatalytic properties of vanadium doped zinc oxide aerogel nanopowder, Thin Solid Films 519 (2011) 5792–5795.
[103] T. Tsuzuki, Z. Smith, A. Parker, R.L. He, X.G. Wang, Photocatalytic activity of manganese-doped ZnO nanocrystalline powders, J. Aust. Ceramic Soc. 45 (2009) 58–62.
[104] B. Donkova, D. Dimitrov, M. Kostadinov, E. Mitkova, D. Mehandjiev, Catalytic and photocatalytic activity of lightly doped catalysts M:ZnO (M = Cu, Mn), Mater. Chem. Phys. 123 (2010) 563–568.
[105] R. Ullah, J. Dutta, Photocatalytic degradation of organic dyes with manganese-doped ZnO nanoparticles, J. Hazard. Mater. 156 (2008) 194–200.
[106] P. Pawinrat, O. Mekasuwandumrong, J. Panpranot, Synthesis of Au–ZnO and Pt–ZnO nanocomposites by one-step flame spray pyrolysis and its application for photocatalytic degradation of dyes, Catal. Commun. 10 (2009) 1380–1385.
[107] S.H. Cho, J.W. Jang, J.S. Lee, K.H. Lee, Carbon-doped ZnO nanostructures synthesized using vitamin C for visible light photocatalysis, Cryst. Eng. Comm. 12 (2010) 3929–3925.
[108] S.W. Liu, C. Li, J.G. Yu, Q.J. Xiang, Improved visible-light photocatalytic activity of porous carbon self-doped ZnO nanosheet-assembled flowers, Cryst. Eng. Comm. 13 (2011) 2533–2541.
[109] D. Li, H. Haneda, Synthesis of nitrogen-containing ZnO powders by spray pyrolysis and their visible-light photocatalysis in gas-phase acetaldehyde decomposition, J. Photochem. Photobiol. A: Chem. 155 (2003) 171–178.
[110] S.F. Chen, W. Zhao, S.J. Zhang, W. Liu, Preparation, characterization and photocatalytic activity of N-containing ZnO powder, Chem. Eng. J. 148 (2009) 263–269.
[111] S. Ahmad, M. Kharkwal, Govind, R. Nagarajan, Application of $KZnF_3$ as a single source precursor for the synthesis of nanocrystals of ZnO_2:F and ZnO:F; synthesis, characterization, optical, and photocatalytic properties, J. Phys. Chem. C 115 (2011) 10131–10139.
[112] F.B. Bouaifel, B. Sieber, N. Bezzi, J. Benner, P. Roussel, L. Boussekey, S. Szunerits, R. Boukherroub, Synthesis and photocatalytic activity of iodine-doped ZnO nanoflowers, J. Mater. Chem. 21 (2011) 10982–10989.
[113] L.Y. Yang, S.Y. Dong, J.H. Sun, J.L. Feng, Q.H. Wu, S.P. Sun, Microwave-assisted preparation, characterization and photocatalytic properties of a dumbbell-shaped ZnO photocatalyst, J. Hazard. Mater. 179 (2010) 438–443.
[114] A. Akyol, M. Bayramoğlu, Photocatalytic degradation of Remazol Red F3B using ZnO catalyst, J. Hazard. Mater. 124 (2005) 241–246.
[115] M.A. Behnajady, S.G. Moghaddam, N. Modirshahla, M. Shokri, Investigation of the effect of heat attachment method parameters at photocatalytic activity of immobilized ZnO nanoparticles on glass plate, Desalination 249 (2009) 1371–1376.
[116] J.C. Sin, S.M. Lam, A.R. Mohamed, Optimizing photocatalytic degradation of phenol by TiO_2/GAC using response surface methodology, Korean J. Chem. Eng. 28 (2011) 84–92.
[117] C.M. So, M.Y. Cheng, J.C. Yu, P.K. Wong, Degradation of azo dye Procion Red MX-5B by photocatalytic oxidation, Chemosphere 46 (2002) 905–912.

[118] M. Sleiman, D. Vildozo, C. Ferronato, J.M. Chovelon, Photocatalytic degradation of azo dye Metanil Yellow: Optimization and kinetic modeling using a chemometric approach, Appl. Catal. B: Environ. 77 (2007) 1–11.
[119] S.M. Lam, J.C. Sin, A.R. Mohamed, Parameter effect on photocatalytic degradation of phenol using TiO_2-P25/activated carbon (AC), Korean J. Chem. Eng. 27 (2010) 1109–1116.
[120] J. Wang, J. Li, Y.P. Xie, C.W. Li, G.X. Han, L.Q. Zhang, R. Xu, X.D. Zhang, Investigation on solar photocatalytic degradation of various dyes in the presence of Er^{3+}:$YAlO_3$/ZnO–TiO_2 composite, J. Environ. Manage. 91 (2010) 677–684.
[121] M.H. Habibi, Photocatalytic mineralisation of four model azo dyes in the presence of nanocomposite thin film Pt-ZnO catalysts coated on glass from aquatic environment, Int. J. Environ. Studies 67 (2010) 393–403.
[122] Y.H. Tong, J. Cheng, Y.L. Liu, G.G. Siu, Enhanced photocatalytic performance of ZnO hierarchical nanostructures synthesized via a two-temperature aqueous solution route, Scripta Mater. 60 (2009) 1093–1096.
[123] J.H. Sun, S.Y. Dong, Y.K. Wang, S.P. Sun, Preparation and photocatalytic property of a novel dumbbell-shaped ZnO microcrystal photocatalyst, J. Hazard. Mater. 172 (2009) 1520–1526.
[124] H.H. Wang, C.S. Xie, W. Zhang, S.Z. Cai, Z.H. Yang, Y.H. Gui, Comparison of dye degradation efficiency using ZnO powders with various size scales, J. Hazard. Mater. 141 (2007) 645–652.
[125] R. Rajeswari, S. Kanmani, Comparative study on photocatalytic oxidation and photolytic ozonation for the degradation of pesticide wastewater, Desalin. Water Treat. 19 (2010) 301–306.
[126] P. Bansal, N. Bhullar, D. Sud, Studies on photodegradation of malachite green using TiO_2/ZnO photocatalyst, Desalin. Water Treat. 12 (2009) 108–113.
[127] U.G. Akpan, B.H. Hameed, Parameters affecting the photocatalytic degradation of dyes using TiO_2-based photocatalysts: A review, J. Hazard. Mater. 170 (2009) 520–529.
[128] S. Merabet, A. Bouzaza, D. Wolbert, Photocatalytic degradation of indole in a circulating upflow reactor by UV/TiO_2 process-influence of some operating parameters, J. Hazard. Mater. 166 (2006) 1244–1249.
[129] B. Krishnakumar, M. Swaminathan, Influence of operational parameters on photocatalytic degradation of a genotoxic azo dye Acid Violet 7 in aqueous ZnO suspensions, Spectrochim. Acta Part A: Mol. Biomol. Spectrosc. 81 (2011) 739–744.
[130] M.A. Behnajady, N. Modirshahla, R. Hamzavi, Kinetic study on photocatalytic degradation of CI Acid Yellow 23 by ZnO photocatalyst, J. Hazard. Mater. 133 (2006) 226–232.
[131] J. Wang, Y.P. Xie, Z.H. Zhang, J. Li, X. Chen, L.Q. Zhang, R. Xu, X.D. Zhang, Photocatalytic degradation of organic dyes with Er^{3+}:$YAlO_3$/ZnO composite under solar light, Solar Energy Mater. Solar Cells 93 (2009) 355–361.
[132] N. Daneshvar, M.H. Rasoulifard, A.R. Khataee, F. Hosseinzadeh, Removal of CI Acid Orange 7 from aqueous solution by UV irradiation in the presence of ZnO nanopowder, J. Hazard. Mater. 143 (2007) 95–101.
[133] C.C. Chen, J.F. Liu, P. Liu, B.H. Yu, Investigation of photocatalytic degradation of methyl orange by using nano-sized ZnO catalysts, Adv. Chem. Eng. Sci. 1 (2011) 9–14.
[134] K. Byrappa, A.K. Subramani, S. Ananda, K.M.L. Rai, R. Dinesh, M. Yoshimura, Photocatalytic degradation of Rhodamine B dye using hydrothermally synthesized ZnO, Bull. Mater. Sci. 29 (2006) 433–438.
[135] A.N. Rao, B. Sivasankar, V. Sadasivam, Kinetic studies on the photocatalytic degradation of direct yellow 12 in the presence of ZnO catalyst, J. Mol. Catal. A: Chem. 306 (2009) 77–81.
[136] G. Annadurai, T. Sivakumar, S. Rajesh Babu, Photocatalytic decolorization of congo red over ZnO powder using Box-Behnken design of experiments, Bioprocess Biosyst. Eng. 23 (2000) 167–173.
[137] K. Hayat, M.A. Gondal, M.M. Khaled, S. Ahmed, Kinetic study of laser-induced photocatalytic degradation of dye (alizarin yellow) from wastewater using nanostructured ZnO, J. Environ. Sci. Health, Part A 45 (2010) 1413–1420.
[138] P. Bansal, D. Sud, Photodegradation of commercial dye, Procion Blue HERD from real textile wastewater using nanocatalysts, Desalination 267 (2011) 244–249.
[139] W.G. Xu, S.F. Liu, S.X. Lu, S.Y. Kang, Y. Zhou, H.F. Zhang, Photocatalytic degradation in aqueous solution using quantum-sized ZnO particles supported on sepiolite, J. Colloid Interf. Sci. 351 (2010) 210–216.
[140] S. Amisha, K. Selvam, N. Sobana, M. Swaminathan, Photomineralisation of Reactive Black 5 with ZnO using solar and UV-A light, J. Korean Chem. Soc. 52 (2008) 66–72.
[141] M.A. Behnajady, N. Modirshahla, M. Shokri, A. Zeininezhad, H.A. Zamani, Enhancement photocatalytic activity of ZnO nanoparticles by silver doping with optimization of photodeposition method parameters, J. Environ. Sci. Health, Part A 44 (2009) 666–672.
[142] R. Kitture, S.J. Koppikar, R. Kaul-Ghanekar, S.N. Kale, Catalyst efficiency, photostability and reusability study of ZnO nanoparticles in visible light for dye degradation, J. Phys. Chem. Solids 72 (2011) 60–66.
[143] S. Ahmed, M.G. Rasul, W.N. Martens, R. Brown, M.A. Hashib, Heterogeneous photocatalytic degradation of phenols in wastewater: A review on current status and developments, Desalination 261 (2010) 3–18.
[144] S.K. Kansal, A.H. Ali, S. Kapoor, Photocatalytic decolorization of biebrich scarlet dye in aqueous phase using different nanophotocatalysts, Desalination 259 (2010) 147–155.
[145] Q. Xiao, J. Zhang, C. Xiao, X.K. Tan, Photocatalytic decolorization of methylene blue over $Zn_{1-x}Co_xO$ under visible light irradiation, Mater. Sci. Eng. B 142 (2007) 121–125.
[146] J. Zhai, X. Tao, Y. Pu, X.F. Zeng, X.F. Chen, Core/shell structured ZnO/SiO_2 nanoparticles: Preparation, characterization and photocatalytic property, Appl. Surf. Sci. 257 (2010) 393–397.
[147] M. Movahedi, A.R. Mahjoub, S. Janitabar-Darzi, Photodegradation of congo red in aqueous solution on ZnO as an alternative catalyst to TiO_2, J. Iran. Chem. Soc. 6 (2009) 570–577.
[148] C.H. Wu, Effects of sonication on decolorization of CI Reactive Red 198 in UV/ZnO system, J. Hazard. Mater. 153 (2008) 1254–1261.
[149] B. Shahmoradi, K. Namratha, K. Byrappa, K. Soga, S. Ananda, R. Somashekar, Enhancement of the photocatalytic activity of modified ZnO nanoparticles with manganese additive, Res. Chem. Intermed. 37 (2011) 329–340.
[150] D.F. Ollis, E. Pelizzetti, N. Serpone, Photocatalyzed destruction of water contaminants, Environ. Sci. Tech. 25 (1991) 1522–1529.
[151] K. Mehrotra, G.S. Yablonsky, A.K. Ray, Macro kinetic studies for photocatalytic degradation of benzoic acid in immobilized systems, Chemosphere 60 (2005) 1427–1436.
[152] A.R. Khataee, M. Zarei, Photocatalysis of a dye solution using immobilized ZnO nanoparticles combined with photoelectrochemical process, Desalination 273 (2011) 453–460.
[153] H.C. Yatmaz, A. Akyol, M. Bayramoglu, Kinetics of the photocatalytic decolorization of an azo reactive dye in aqueous ZnO suspensions, Ind. Eng. Chem. Res. 43 (2004) 6035–6039.
[154] M.A. Behnajady, N. Modirshahla, N. Daneshvar, M. Rabbani, Photocatalytic degradation of CI Acid Red 27 by immobilized ZnO on glass plates in continuous-mode, J. Hazard. Mater. 140 (2007) 257–263.
[155] K. Byrappa, A.K. Subramani, S. Ananda, K.M.L. Rai, M.H. Sunitha, B. Basavalingu, K. Soga, Impregnation of ZnO onto activated carbon under hydrothermal conditions and its photocatalytic properties, J. Mater. Sci. 41 (2006) 1355–1362.
[156] C. Guillard, E. Puzenat, H. Lachheb, A. Houas, J.M. Herrmann, Why inorganic salts decrease the TiO_2 photocatalytic efficiency, Int. J. Photoenergy 7 (2005) 1–9.

[157] N. Kashif, F. Ouyang, Parameters effect on heterogeneous photocatalysed degradation of phenol in aqueous dispersion of TiO_2, J. Environ. Sci. 21 (2009) 527–533.
[158] M.L. Zhang, T.C. An, X.H. Hu, C. Wang, G.Y. Sheng, J.M. Fu, Preparation and photocatalytic properties of a nanometer ZnO–SnO_2 coupled oxide, Appl. Catal. A: Gen. 260 (2004) 215–222.
[159] B. Krishnakumar, M. Swaminathan, Solar photocatalytic degradation of Acid Black 1 with ZnO, Indian J. Chem. 49A (2010) 1035–1040.
[160] S. Bhandari, J. Vardia, R.K. Malkani, S.C. Ameta, Effect of transition metal ions on photocatalytic activity of ZnO in bleaching of some dyes, Toxicol. Environ. Chem. 88 (2006) 35–44.
[161] L.S. Roselin, G.R. Rajarajeswari, R. Selvin, V. Sadasivam, B. Sivasankar, K. Rengaraj, Photocatalytic oxidation of AV 19: Mechanistic aspects involving primary oxidizing species, React. Kinet. Catal. Lett. 78 (2003) 259–265.
[162] M.L. Chin, A.R. Mohamed, S. Bhatia, Performance of photocatalytic reactors using immobilized TiO_2 film for the degradation of phenol and methylene blue dye present in water stream, Chemosphere 57 (2004) 547–554.
[163] M.L. Zhang, T.C. An, J.M. Fu, G.Y. Sheng, X.M. Wang, X.H. Hu, X.J. Ding, Photocatalytic degradation of mixed gaseous carbonyl compounds at low level on adsorptive TiO_2/SiO_2 photocatalyst using a fluidized bed reactor, Chemosphere 64 (2006) 423–431.
[164] S.I. Abou-Elela, M.A. El-Khateeb, Treatment of ink wastewater via heterogeneous photocatalytic oxidation, Desalin. Water Treat. 7 (2009) 1–5.
[165] S. Adishkumar, S. Kanmani, Treatment of phenolic wastewaters in single baffle reactor by solar/TiO_2/H_2O_2 process, Desalin. Water Treat. 24 (2010) 67–73.
[166] B. Pare, P. Singh, S.B. Jonnalgadda, Artificial light assisted photocatalytic degradation of lissamine fast yellow dye in ZnO suspension in a slurry batch reactor, Indian J. Chem. 48A (2009) 1364–1369.
[167] A. Habib, I.M.I. Ismail, A.J. Mahmood, R. Ullah, Photocatalytic decolorization of Brilliant Golden Yellow in TiO_2 and ZnO suspensions. J. Saudi Chem. Soc., Corrected Proof available online 22 February 2011 (2011).
[168] R. Suárez-Parra, I. Hernández-Pérez, M.E. Rincón, S. López-Ayala, M.C. Roldán-Ahumada, Visible light-induced degradation of blue textile azo dye on TiO_2/CdO–ZnO coupled nanoporous films, Solar Energy Mater. Solar Cells 76 (2003) 189–199.
[169] N. Sobana, M. Swaminathan, The effect of operational parameters on the photocatalytic degradation of acid red 18 by ZnO, Sep. Purif. Technol. 56 (2007) 101–107.
[170] Z.M. Zhang, H.L. Zheng, Optimization for decolorization of azo dye acid green 20 by ultrasound and H_2O_2 using response surface methodology, J. Hazard. Mater. 172 (2009) 1388–1393.
[171] C. Lizama, J. Freer, J. Baeza, H.D. Mansilla, Optimized photodegradation of Reactive Blue 19 on TiO_2 and ZnO suspensions, Catal. Today 76 (2002) 235–246.
[172] U.I. Gaya, A.H. Abdullah, Z. Zainal, M.Z. Hussein, Photocatalytic treatment of 4-chlorophenol in aqueous ZnO suspensions: Intermediates, influence of dosage and inorganic anions, J. Hazard. Mater. 168 (2009) 57–63.
[173] B.K. Körbahti, M.A. Rauf, Application of response surface analysis to the photolytic degradation of Basic Red 2 dye, Chem. Eng. J. 138 (2008) 166–171.
[174] Y.F. Gao, M. Nagai, Y. Masuda, F. Sato, K. Koumoto, Electrochemical deposition of ZnO film and its photoluminescence properties, J. Cryst. Growth 286 (2006) 445–450.
[175] S. Li, S. Meierott, J.M. Köhler, Effect of water content on growth and optical properties of ZnO nanoparticles generated in binary solvent mixtures by micro-continuous flow synthesis, Chem. Eng. J. 165 (2010) 958–965.
[176] L. Zhao, J.S. Lian, Y.H. Liu, Q. Jiang, Influence of preparation methods on photoluminescence properties of ZnO films on quartz glass, Trans. Nonferrous Met. Soc. China 18 (2008) 145–149.
[177] H.Y. Bae, G.M. Choi, Electrical and reducing gas sensing properties of ZnO and ZnO–CuO thin films fabricated by spin coating method, Sensors Actuators B 55 (1999) 47–54.
[178] A.N. Gruzintsev, V.T. Volkov, C. Barthou, P. Benalloul, J.M. Frigerio, Stimulated emission from ZnO–SiO_2–Si thin film nanoresonators obtained by magnetron sputtering method, Thin Solid Films 459 (2004) 262–266.
[179] C.Q. Ge, C.S. Xie, S.Z. Cai, Preparation and gas-sensing properties of Ce-doped ZnO thin-film sensors by dip-coating, Mater. Sci. Eng. B 137 (2007) 53–58.
[180] S. Fernández, O.D. Abril, F.B. Naranjo, J.J. Gandía, High quality textured ZnO:Al surfaces obtained by a two-step wet-chemical etching method for applications in thin film silicon solar cells, Solar Energy Mater. Solar Cells 95 (2011) 2281–2286.
[181] W.S. Ning, H.Y. Shen, H.Z. Liu, Study of the effect of preparation method on CuO–ZnO–Al_2O_3 catalyst, Appl. Catal. A: Gen. 211 (2001) 153–157.
[182] J. Li, H.Q. Fan, X.P. Chen, Z.Y. Cao, Structural and photoluminescence of Mn-doped ZnO single-crystalline nanorods grown via solvothermal method, Colloids Surf. A: Physiochem. Eng. Aspects 349 (2009) 202–206.
[183] X.L. Zong, P. Wang, Effect of UV irradiation on the properties of ZnO nanorod arrays prepared by hydrothermal method, Physica E 41 (2009) 757–761.
[184] S.K.L. Devi, K.S. Kumar, A. Balakrishnan, Rapid synthesis of pure and narrowly distributed Eu doped ZnO nanoparticles by solution combustion method, Mater. Lett. 65 (2011) 35–37.
[185] S.K. Lim, S.H. Hwang, S. Kim, Microemulsion synthesis and characterization of aluminum doped ZnO nanorods, Cryst. Res. Technol. 45 (2010) 771–775.
[186] H.C. Cheng, C.F. Chen, C.Y. Tsay, J.P. Leu, High oriented ZnO films by sol–gel and chemical bath deposition combination method, J. Alloys Compounds 475 (2009) L46–L49.
[187] K.E. Kim, S.R. Jang, J.H. Park, R. Vittal, K.J. Kim, Enhancement in the performance of dye-sensitized solar cells containing ZnO-covered TiO_2 electrodes prepared by thermal chemical vapor deposition, Solar Energy Mater. Solar Cells 91 (2007) 366–370.
[188] X. Zhang, H.L. Zhao, X.J. Tao, Y.B. Zhao, Z.J. Zhang, Sonochemical method for the preparation of ZnO nanorods and trigonal-shaped ultrafine particles, Mater. Lett. 59 (2005) 1745–1747.
[189] S.C. Lyu, Y. Zhang, C.J. Lee, H. Ruh, H.J. Lee, Low-temperature growth of ZnO nanowire array by a simple physical vapor-deposition method, Chem. Mater. 15 (2003) 3294–3299.
[190] J. Zhou, Z.D. Wang, L. Wang, M. Wu, S.X. Ouyang, E. Gu, Synthesis of ZnO hexagonal tubes by a microwave heating method, Superlattices Microstructures 39 (2006) 314–318.
[191] K. Hayat, M.A. Gondal, M.M. Khaled, S. Ahmed, A.M. Shemsi, Nano ZnO synthesis by modified sol gel method and its application in heterogeneous photocatalytic removal of phenol from water, Appl. Catal. A: Gen. 393 (2011) 122–129.
[192] S. Bandyopadhyay, G.K. Paul, R. Roy, S.K. Sen, S. Sen, Study of structural and electrical properties of grain-boundary modified ZnO films prepared by sol–gel technique, Mater. Chem. Phys. 74 (2002) 83–91.
[193] M. Muruganandham, I.S. Chen, J.J. Wu, Effect of temperature on the formation of macroporous ZnO bundles and its application in photocatalysis, J. Hazard. Mater. 172 (2009) 700–706.
[194] O. Mekasuwandumrong, P. Pawinrat, P. Praserthdam, J. Panpranot, Effects of synthesis conditions and annealing post-treatment on the photocatalytic activities of ZnO nanoparticles in the degradation of methylene blue dye, Chem. Eng. J. 164 (2010) 77–84.

[195] S. Su, S.X. Lu, W.G. Xu, Photocatalytic degradation of reactive brilliant blue X-BR in aqueous solution using quantum-sized ZnO, Mater. Res. Bull. 43 (2008) 2172–2178.
[196] E. Yassitepe, H.C. Yatmaz, C. Öztürk, K. Öztürk, C. Duran, Photocatalytic efficiency of ZnO plates in degradation of azo dye solutions, J. Photochem. Photobio. A: Chem. 198 (2008) 1–6.
[197] C.A.K. Gouvêa, F. Wypych, S.G. Moraes, N. Durán, P. Peralta-Zamora, Semiconductor-assisted photodegradation of lignin, dye, and kraft effluent by Ag-doped ZnO, Chemosphere 40 (2000) 427–432.
[198] I. Poulios, E. Micropoulou, R. Panou, E. Kostopoulou, Photooxidation of eosin Y in the presence of semiconducting oxides, Appl. Catal. B: Environ. 41 (2003) 345–355.
[199] D.P. Mohapatra, K. Brar, R.D. Tyagi, R.Y. Surampalli, Physico-chemical pre-treatment and biotransformation of wastewater and wastewater sludge—fate of bisphenol A, Chemosphere 78 (2010) 923–941.
[200] J. Sajiki, Decomposition of BPA by radical oxygen, J. Environ. Int. 27 (2001) 315–320.
[201] M.A. Barakat, Adsorption and photodegradation of Procion yellow H-EXL dye in textile wastewater over TiO_2 suspension, J. Hydro-Environ. Res. 5 (2011) 137–142.
[202] S.K. Kansal, M. Singh, D. Sud, Effluent quality at kraft/soda agro-based paper mills and its treatment using a heterogeneous photocatalytic system, Desalination 228 (2008) 183–190.
[203] L.S. Roselin, R. Selvin, Photocatalytic treatment and reusability of textile dyeing effluents from cotton dyeing industries, Sci. Adv. Mater. 3 (2011) 113–119.
[204] H.P. Shivaraju, K. Byrappa, M.B. Shayan, T. Rungnapa, S. Pakamard, V. Kumar, S. Ananda, Hydrothermal coating of ZnO onto calcium alumino silicate beads and their application in photodegradation of amaranth dye, Mater. Res. Innov. 14 (2010) 73–79.
[205] E.R. Bandala, C.A. Arancibia-Bulnes, S.L. Orozco, C.A. Estrada, Solar photoreactors comparison based on oxalic acid photocatalytic degradation, Sol. Energy 77 (2004) 503–512.
[206] R.J. Braham, A.T. Harris, Review of major design and scale-up considerations for solar photocatalytic reactors, Ind. Eng. Chem. Res. 48 (2009) 8890–8905.
[207] C. Singh, R. Chaudhary, R.S. Thakur, Performance of advanced photocatalytic detoxification of municipal wastewater under solar radiation—a mini review, Int. J. Energy Environ. 2 (2011) 337–350.
[208] A.R. Khataee, Optimization of UV-promoted peroxydisulphate oxidation of CI Basic Blue 3 using response surface methodology, Environ. Technol. 31 (2010) 73–86.
[209] A.R. Khataee, M. Fathinia, S. Aber, M. Zarei, Optimization of photocatalytic treatment of dye solution on supported TiO_2 nanoparticles by central composite design: Intermediates identification, J. Hazard. Mater. 181 (2010) 886–897.